

A bicycle can be balanced by stochastic optimal feedback control

Eric Maris*

**Donders Institute for Brain, Cognition, and Behaviour, Radboud University,
Nijmegen, The Netherlands*

Corresponding Author:

e-mail: eric.maris@donders.ru.nl (EM)

Abstract

I propose and evaluate a model for bicycle balance control. The central concept in this model is a computational system, implemented in the central nervous system (CNS), that not only controls but also learns a mechanical system that exists outside the CNS. This computational system uses an internal model to calculate optimal control actions as specified by stochastic optimal control theory. Because the computational system depends on parameters that the CNS must learn from interaction with the mechanical system, this model must be robust against inaccuracies in the learned parameter values. By means of simulations, I demonstrate that this model can balance a bicycle under realistic conditions and is robust against some (but not all) variations in the learned noise characteristics. The model is not robust to variations in the learned internal model caused by a misestimation of the speed. Although the current model makes several simplifications for the sake of computational feasibility, it can be extended in several directions to provide a more realistic account of human balance control.

Keywords

sensorimotor control, balance, bicycle balance, internal model, stochastic optimal feedback control, linear quadratic Gaussian, motor learning

Author summary

Balancing a bicycle is typical for the balance control humans perform as a part of a whole range of behaviors (walking, running, skating, skiing, etc.). This paper presents a general model of balance control and applies it to the balancing of a bicycle. Understanding balance control has both a physics (mechanics) and a neurobiological component. The physics component pertains to the laws that govern the movements of the rider and his bicycle, and the neurobiological component pertains to the mechanisms via which the central nervous system (CNS) learns these physics laws and uses this for balance control. This paper presents a computational model of this neurobiological component. The central concept in this model is a computational system, implemented in the CNS, that uses an internal model to calculate optimal control actions. Because this computational system depends on parameters that the CNS must learn from interaction with the environment (i.e., the body that is attached to the CNS and the bicycle), this model must be robust against inaccuracies in the learned parameter values. By means of simulations, I demonstrate that this model can balance a bicycle under realistic conditions and is robust against some (but not all) variations in the learned noise characteristics. The model is not robust to variations in the learned internal model caused by a misestimation of the speed. This implies that the CNS must implement a mechanism for accurate speed estimation and selection of the appropriate internal model.

Introduction

Keeping balance is an important function for many organisms. Most likely, it is related to the organisms' ability to move, as this imposes the requirement to control one body axis relative to gravity. In this paper, I will focus on balancing a bicycle. However, much of what I will say also holds for other forms of balancing that involve a human body: walking, running, skating, skiing, etc. For example, all forms of balancing a human body involve the same two basic actions for keeping the body's center of mass (CoM) above its area of support (AoS): (1) shifting the CoM while keeping the AoS more or less fixed (e.g., by leaning the upper body), and (2) changing the AoS while keeping the CoM more or less fixed (e.g., by stepping out with one leg).

Keeping balance is a sensorimotor control problem: the central nervous system (CNS) receives sensory information about the body, the body-attached tools (bicycle, skates, skis, ...), and their environment (turn radius, speed, ...), and uses this information for calculating actions with which it controls their position relative to gravity. The dominant model for sensorimotor control assumes that the CNS makes use of an internal model to determine these control actions [1, 2]. In some publications [3, 4], a distinction is made between forward and inverse internal models, but here I will only consider forward models; the inverse model will be denoted as the feedback control law. The (forward) internal model simulates the dynamics of the plant (body plus body-attached tools) it attempts to control.

A very influential version of this model claims that this control is optimal in the sense that it minimizes a cost functional that depends on movement precision (here, deviation from the upright position) and energetic costs [1, 2]. This model is called optimal feedback control (OFC), and in this paper I will apply the stochastic version of OFC to bicycle balance control; the deterministic version would predict that the CoM stays exactly above the AoS once this position is reached, which is unrealistic.

To evaluate the plausibility of stochastic OFC as a model for bicycle balance control, one must address at least the following questions: (1) Is the model good enough to balance a bicycle under realistic conditions (lean and steering angles and angular rates that are observed with real riders), and (2) Is the model robust against variations in the parameter values that the CNS must learn? The relevance of robustness follows from the fact that every internal model has parameters (gain factors, moment arms, ...) that the CNS must learn from experience with the plant. In the optimal scenario these values allow for the most accurate simulation of the plant dynamics. However, in the beginning of the learning process, these parameter values cannot be very close to their optimal values, and therefore the model must have some minimal robustness against variations in these parameter values. Of course, the stabilization performance (indexed by, e.g., lean angle variability) may depend on these parameter values, but for a realistic range of values (see *Results*), the simulated bicycle should not fall over.

In the remainder of this introduction, I will first describe the mechanical aspects of bicycle balance control, and next how bicycle balance control can be formulated as a stochastic optimal control problem. In the Results section, I will first introduce a model of sensorimotor control that is based on the idea that a mechanical system is both controlled and learned by a computational system that uses an internal model to calculate optimal control actions. Next, in a simulation study, I will evaluate (1) whether this model is good enough to balance a bicycle under realistic conditions, and (2) whether it is robust to variations in the values of two types of learned parameters of the computational system.

Control actions for balancing a bicycle

Problem definition

A standing human is balanced when his center of mass (CoM) is above his base of support (BoS), which is formed by the soles of his two feet plus the area in between. Balance follows from the fact that the direction of the gravitational force (a vector quantity in 3D passing through the CoM) intersects this BoS. The situation is similar but not identical for a bicycle. A stationary bicycle (i.e., a

bicycle in a track stand) is balanced when the combined CoM of rider and bicycle is above the one-dimensional line of support (LoS), the line that connects the contact points of the two wheels with the road surface. In this position, the direction of the gravitational force intersects the LoS. However, because of disturbances, the CoM cannot be exactly above this one-dimensional LoS for a finite period of time. Therefore, a bicycle is considered balanced if the CoM fluctuates around the LoS within a limited range, small enough to prevent the bicycle from touching the road surface.

Compared to a stationary bicycle, the balance of a moving bicycle is more complicated because, besides gravity, also the centrifugal force acts on the CoM. Crucially, the centrifugal force is under the rider's control via the turn radius [5]. The balance of a moving bicycle depends on the resultant of all forces that act on the CoM: a bicycle is balanced if the direction of this resultant force fluctuates around the LoS within a fixed range. Besides the forces that act on the CoM, there are also forces that are responsible for the turning of the bicycle's front frame, and some of these do not depend on the rider [6]. These latter forces are responsible for the bicycle's self-stability and will be discussed later (see *Bicycle self-stability*).

The geometry of the rider-bicycle combination

The control actions with which a rider can balance his bicycle are constrained by the geometry of the bicycle and the rider's position on it. To describe the possible control actions, I start from the kinematic variables of a model of the rider-bicycle combination, shown in Figure 1. This model consists of three rigid bodies: front frame, rear frame, and the rider's upper body. The positions of these three bodies are specified by three angular variables: (1) the steering angle (the position of the front frame relative to the rear frame, denoted by δ), (2) the rear frame lean angle (the position of the rear frame relative to gravity, denoted by θ_1), and (3) the upper body lean angle (the position of the upper body relative to gravity, denoted by θ_2).

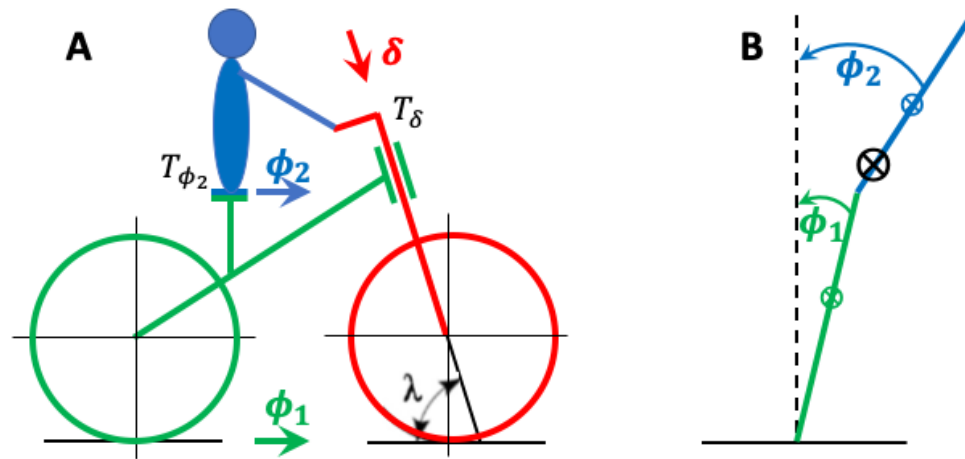


Figure 1: Kinematic variables of the bicycle model plus the rider-controlled torques. (A) Side view. In green, the bicycle rear frame, characterized by its lean angle ϕ_1 over the roll axis (green arrow). In red, the bicycle front frame, characterized by its angle δ over the steering axis (red arrow). In blue, the rider's upper body, characterized by its lean angle ϕ_2 over the roll axis (blue arrow). In black, (1) the steering torque T_{δ} and the lean torque T_{ϕ_2} , which are both applied by the rider, and (2) the steering axis angle λ , which is set equal to 90 degrees for the purposes of the present paper (see text). (B) Rear view. In green, the bicycle rear frame (plus lower body) lean angle ϕ_1 (which is equals the front frame lean angle). In blue, the rider's upper body lean angle ϕ_2 . The symbol \otimes denotes the CoG of the upper body (in blue), the lower body (in green), and combined (in black).

I assume that the rider sits on the saddle, does not pedal, and keeps his feet resting on the non-moving pedals. In this setup, the rider's lower body (the hips and below) is firmly supported, and can be considered a part of the rear frame. This simplification does not prevent using this bicycle model for investigating the effect of pedaling-related movements on balance control, for which there is good evidence [7]. This simplification only implies that leg movements cannot be used for balance control. Thus, the only forces that can be used for balance control are (1) a steering torque T_{δ} on the handlebars, and (2) a lean torque T_{ϕ_2} at the hinge between the rider's upper body and the rear frame, corresponding to the hips.

Cycling involves a double balance problem

Cycling involves a double balance problem, of which I have already described the first part: keeping the combined CoG of the rider and the bicycle above the LoS. The second balance problem only pertains to the rider's upper body: keeping the CoG of this upper body above its BoS, which is the saddle. I simplify this balance problem by only considering the balance over the roll axis (parallel to the LoS), which corresponds to upper body movements to the left and the right. I thus ignore the balance over the pitch axis (perpendicular to the LoS and gravity), which corresponds to upper body movements to the front and the back, typically caused by accelerations and braking. With this simplification, the joint between the rider's upper body and the rear frame is a hinge with a single degree of freedom.

Balance control strategies from a mechanical point of view

For keeping the combined CoG over the LoS (the first balance problem), the relevant control actions must result in a torque over the LoS (roll axis). Within the constraints of our kinematic model, there are two ways for a rider to perform a control action: (1) by turning the handlebars, and (2) by leaning the upper body. To explain these control actions, it is convenient to make use of Figure 1B. This is the schematic of a double compound pendulum, of which the dynamics depend on how it is actuated: (1) if the contact between the green rod and the road surface is actuated by a linear force, the dynamics is known as the “double compound pendulum on a cart” [8], and (2) if the angle between the green and the blue rod (the upper body lean angle) is controlled by a torque at this joint (the hips), the dynamics is known as the Acrobot [9].

We first take the perspective of a double compound pendulum on a cart, which involves that, by turning the handlebars, the contact point of the green rod (representing the combined front and rear frame) with the road surface moves to the right under the combined CoG. In fact, turning the handlebars changes the trajectory of the tire-road contact points and, because the CoM wants to continue

in its pre-turn direction (by Newton's first law), this results in a centrifugal force in the bicycle reference frame (of which the LoS is one of the defining axes; the roll axis). This centrifugal force is perpendicular to the LoS and this results in a torque over the roll axis in the direction opposite to the turn (a tipping out torque). This steering-induced tipping out torque can be used to move the combined CoG to the opposite side of the turn. Thus, steering in the direction of the lean produces a tipping out torque that brings the combined CoG over the LoS. This explains this control mechanism's name: "steering to the lean".

We now take the perspective of the Acrobot, which involves that, by applying a lean torque at the hips, the lean angles of both body parts change. As a consequence, the separate CoGs of both body parts are shifted, and this in turn affects the gravity-dependent torques on these body parts. Crucially, a lean torque at the hips does not shift the combined CoG, and therefore cannot bring this combined CoG above the LoS in a direct way. However, it can do so in an indirect way, namely by turning the front frame. This is essential for the mechanism via which a bicycle can be balanced when riding no-handed. First, when leaning the upper body sufficiently to one side, the bicycle and the lower body lean to the other side. Next, depending on properties of the bicycle (wheel flop, the wheels' gyroscopic forces, the combined CoG [6, 10]), leaning the bicycle to one side turns the front frame to the same side. This lean-induced turn of the front frame then initiates the same mechanism as when turning the front frame by means of the handlebars: a change in the trajectory of the tire-road contact points results in a centrifugal force perpendicular to the LoS, producing a torque over the roll axis in the direction opposite to the turn. This lean torque brings the LoS under the CoG.

For the second balance problem (keeping the upper body's CoG over its BoS), the same two control actions can be used: (1) turning the handlebars, and (2) applying a lean torque at the hips. Turning the handlebars in the direction of the upper body lean produces a lean torque in the other direction (i.e., away from the lean), and this allows to control this upper body lean angle. By applying a lean torque at the hips, this upper body lean angle can be controlled in a more direct way, but at the expense of leaning the bicycle (and the lower body) in the opposite direction.

Because the two balance problems use the same control actions, coordination is required. For example, a torque at the hips can be used to counter the turning-induced centrifugal torque on the upper body: by applying a hip torque of equal magnitude as this centrifugal torque (but opposite direction), the position of the upper body can be controlled. There exists an energy-efficient alternative for this upper body control strategy, well-known in motorcycle racing: leaning the upper body to the inside of the turn. When the upper body is sufficiently leaned to the inside of the turn, the resulting gravity-induced torque will counter the centrifugal torque on the upper body CoG.

Balancing and steering

When riding a bicycle, the rider typically does not only want to balance his bicycle, but also wants to steer it over a chosen/indicated trajectory. This paper only considers control actions for balancing the bicycle, and therefore will not consider constraints on the trajectory, such as obstacles and bicycle path edges. This pure balance task corresponds to cycling blindfolded on an empty parking lot. After a brief familiarization, most humans can cycle blindfolded on an empty parking lot; a search on social media will show several demonstrations of this.

Bicycle self-stability

At this point, it is necessary to mention the self-stability of the bicycle, which involves that the bicycle is balanced within a certain range of speeds without control actions by the rider [6]. Self-stability is investigated by modelling the rider as a mass that is rigidly attached to the rear frame and does not touch the front frame, allowing the handlebars to move freely. Self-stability depends on several factors, such as geometric trail, pneumatic trail, wheel flop, the wheels' gyroscopic forces, and the combined CoG [6, 10]. These factors all contribute to the bicycle's tendency to steer in the direction of the lean.

Because the present paper only focuses on the rider's contribution to bicycle stability, from our model bicycle, I removed all known factors that contribute to

the bicycle's self-stability (see Figure 2). Specifically, I removed the effects of pneumatic trail and the wheel's gyroscopic forces by replacing the wheels by ice skates (or, equivalently, tiny roller skate wheels). And I removed the effects of geometric trail and wheel flop by choosing a vertical steering axis (i.e., by setting λ in Figure 1 to 90 degrees), as in most bicycles for BMX and artistic cycling. I also keep the CoG at approximately the same position as on a regular bicycle (i.e., 29 cm before the rear wheel contact point), because a CoG with a more anterior position may result in bicycle self-stability [10]. It is important to observe that, without these effects, the bicycle's front frame does not turn in the direction of the lean unless the rider turns the handlebars. Therefore, the balance control strategy for riding no-handed that I described before, cannot be used on this model bicycle. In the Methods and Models section, I will describe how this simplified bicycle-rider combination can be modeled as a double pendulum of which the base can be moved by turning the front wheel/skate, and the joint at the hips can be actuated. This model will be called the "steered double pendulum" (SDP)

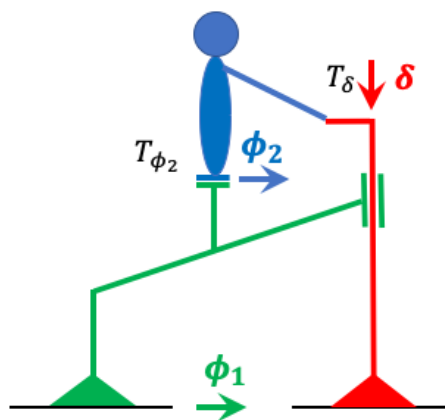


Figure 2: Bicycle model without the known factors that affect bicycle self-stability. Compared to Figure 1, this model has ice skates instead of wheels and a vertical steering axis.

Control and noise forces

For investigating balance control, one must distinguish between control and noise forces. Loosely formulated, control forces are the forces that the rider uses to

balance the bicycle. For a more precise formulation, I adopt the optimal control framework, which defines control actions as the actions that optimize a quantitative performance index. Thus, control forces are the optimal forces for a given performance index.

Noise forces are the difference between the forces that are actually applied and the optimal control forces. It is useful to distinguish between two groups of noise forces: (1) noise forces that originate from the rider, and (2) noise forces that originate from interactions of the bicycle with the environment (e.g., collisions, gusts of wind). In this paper, I only consider noise forces that originate from the rider. These noise forces affect the balance via the same contact points as the two control forces (the handlebars and the saddle). These noise forces are an important instrument in the simulations that I will run to investigate bicycle balance control: they distort the balance, and this allows us to investigate different balance-restoring (stabilizing) mechanisms.

Balancing a bicycle as a stochastic optimal control problem

Optimal feedback control

Every motor task can be performed in an infinite number of ways, and this is for two reasons: (1) the human body has a very large number of joints that can be used in various combinations to produce the same endpoint trajectory, and (2) a motor task unfolds over time and can be performed with different speed profiles. Nevertheless, most motor tasks are performed in a highly stereotyped manner. For instance, reaching tasks consistently show roughly straight-line paths with bell-shaped speed profiles [2].

To explain these highly stereotyped actions among skilled performers, Todorov and colleagues [2, 11] proposed optimal control theory. This theory uses a scalar cost functional that increases with time-integrated imprecisions (inaccuracies) and energetic costs. Optimal control involves that the control actions are chosen such that this cost functional is minimized. There are two versions of optimal control

that differ with respect to how the sensory feedback is used: (1) a version that assumes a fixed planned trajectory and uses sensory feedback to correct for deviations from this planned trajectory [for an overview, see 1], and (2) a version without a planned trajectory in which the control actions are merely a function of the feedback [2, 11-14]. This second version is called optimal feedback control (OFC).

I will propose a model for bicycle balance control based on OFC. In line with OFC, I thus hypothesize that balancing a bicycle does not involve trajectory planning. Importantly, this hypothesis only applies to the specific task of balance control (as when cycling blindfolded on an empty parking lot) and not necessarily to other aspects of cycling, such as steering a bicycle over an indicated trajectory or an obstacle course. For these other aspects, it is likely that some form of trajectory planning is required.

In previous work, OFC has been mainly applied to reaching tasks [1, 11-14]. For such tasks, the overall precision predominantly depends on the precision at the endpoint of the reaching movement. In line with this fact, the cost functional is dominated by imprecisions (distances between the end effector and the reach target) near the endpoint [11]. In contrast, for tasks in which a state must be maintained over time, such as balancing a bicycle, the cost functional must depend on the imprecisions uniformly across the (theoretically) infinite lean angle trajectory.

For applying OFC, one needs the equations of motion (EoM) that describe the dynamics of the system (here, the rider-bicycle combination) as a set of differential equations. The variables of these differential equations are the so-called state variables, and for the SDP they are the following: the steering angle δ , the rear frame lean angle θ_1 , the upper body lean angle θ_2 (see Figure 2), plus their corresponding angular rates. In Appendix A, I will derive the EoM from Lagrangian mechanics.

The EoM for the SDP are nonlinear and this has important implications for using OFC for stabilization (here, bicycle balance control). Specifically, OFC does not

provide general results for stabilizing a nonlinear system. However, it provides very useful results for stabilizing a linear system, and this has led to the common practice in robotics to linearize the nonlinear system, apply OFC for linear systems, and use the resulting optimal control signals to stabilize the nonlinear system [9]. I hypothesize that the CNS implements a similar solution for stabilizing a bicycle and the rider's upper body: build an internal linear approximation of the external nonlinear system that the CNS wants to stabilize, and use calculations similar to those from OFC to achieve this. In a later section, *Stabilizing a nonlinear mechanical system by linear stochastic OFC*, I will describe this model in more detail.

OFC uses a scalar cost functional to define the optimal control actions. Because the CNS implements functions for setting goals and evaluating actions, minimizing a cost functional is a plausible assumption for the CNS. For our application to bicycle balance control, it is natural to define this cost functional as one that increases with (1) deviations from the upright position (for both the bicycle and the upper body), and (2) the energetic costs of the control actions. The control actions that result from the minimization of this cost functional are the steering and the lean torque.

Sensorimotor noise and stochastic OFC

Because riders and other biological systems suffer from sensor and motor noise [15], deterministic OFC is an unrealistic model for bicycle balance control. Sensor and motor noise are responsible for the fact that the CNS cannot perfectly know the world outside of the CNS (which includes the body that is attached to it). Specifically, if the sensory feedback is noisy, the CNS cannot infer the state variables perfectly from this feedback. With respect to the motor noise, one must know that the CNS is unaware of the noise that is generated at the muscular level, because this noise is added after the CNS has produced the motor command. Therefore, even if the CNS was perfectly accurate in calculating the new state that results from its motor commands, the outcome of this calculation would not match with the actual state, because this state is also affected by the motor noise.

Fortunately, for a system whose behavior depends on noise, the control can still be optimal. To define optimality in this stochastic context, the ordinary differential equations (ODEs) are replaced by the corresponding stochastic differential equations (SDEs). If these SDEs are linear, the noise is additive and Gaussian, and the cost functional is quadratic, then control is optimal if it is based on an optimal state estimate [16]. The optimality of this state estimate is relative to the conditional probability distribution of the state estimate at time t given the values of all variables on previous times. Therefore, the optimal estimate not only depends on the sensory feedback at time t , but also on the optimal state estimate and the control action (actually, its efference copy) just before this time. This optimal estimator involves the familiar Kalman filter, which weights the sensory feedback in proportion to its reliability. Several empirical studies have suggested that state estimation in the CNS involves this type of weighting in proportion to the reliability of the information [17-19].

The ability to correct for motor and sensor noise depends on the CNS's internal model of the dynamics of the plant and the sensory feedback. The CNS uses this internal model to estimate the current state from (1) the previous state, (2) the most recent control action, and (3) the sensory feedback. Several psychophysical [20-22] and neurophysiological [23, 24] studies have provided evidence for such internal models. An internal model can be conceived as a set of differential equations that allows the CNS to simulate state variables and to combine this information with the sensory feedback to obtain an optimal state estimate.

The robustness of control based on an internal model

Because the internal model cannot be directly observed, its hypothesized role in sensorimotor control has to be evaluated on the basis of its performance. This performance pertains to how well the optimal controls under a linear approximation can stabilize a nonlinear system. This linear approximation involves several parameters, such as the matrices that define the linear approximation of the nonlinear EoM and the noise covariance matrices (see *Stabilizing a nonlinear mechanical system by linear stochastic OFC*). The larger the range of parameter and state values for which the internal model can stabilize

the nonlinear system, the more robust the control, and the more likely that the CNS uses a similar internal model for sensorimotor control. In this paper, for a few different parameter sets, I will determine the range of values for which the internal model can stabilize the nonlinear system while producing realistic state values. Parameters with wide and narrow ranges correspond to, respectively, the strong and the weak aspects of the internal-model-based control mechanism.

Results

Stabilizing a nonlinear mechanical system by linear stochastic OFC

A model for sensorimotor control

The EoM for most dynamical systems are nonlinear. This holds for the model bicycle, the SDP, but also for common movements such as reaching, throwing, and walking; these movements are all performed by changing joint angles, which results in EoM involving trigonometric functions. I denote the nonlinear EoM as follows:

$$\dot{\mathbf{x}} = \Omega(\mathbf{x}, \mathbf{u})$$

The vector \mathbf{x} contains the state variables, and $\dot{\mathbf{x}}$ their first derivatives with respect to time. For the SDP, $\mathbf{x} = [\delta, \phi_1, \phi_2, \dot{\delta}, \dot{\phi}_1, \dot{\phi}_2]^T$ and $\mathbf{u} = [T_\delta, T_{\phi_2}]^T$ (see Figure 2). In the Methods and Models section, I will derive the SDP EOM from Lagrangian mechanics.

OFC calculates optimal control actions \mathbf{u} that minimize a cost functional $J(\mathbf{x}(\cdot), \mathbf{u}(\cdot))$, in which $\mathbf{x}(\cdot)$ and $\mathbf{u}(\cdot)$ denote the trajectories of, respectively, the state variables and the control actions. Typically, this cost functional increases with the integrated imprecision and energetic costs (e.g., the integrated squared length of $\mathbf{x}(\cdot)$, resp., $\mathbf{u}(\cdot)$; see further). Crucially, this cost functional depends on the EoM, and this raises the important question how the CNS can calculate optimal control actions in the extremely likely scenario that it does not know $\Omega(\mathbf{x}, \mathbf{u})$ exactly. For this scenario, I assume that the CNS learns an approximation to $\Omega(\mathbf{x}, \mathbf{u})$ from experience with the mechanical system. The CNS then uses this approximation as an internal model to estimate the state and calculate the optimal control actions.

In Figure 3, I have depicted a model for sensorimotor control that is based on an internal model that is a linear approximation of the unknown nonlinear dynamics $\Omega(\mathbf{x}, \mathbf{z})$. These nonlinear dynamics are depicted in red, and will be denoted as the mechanical system. In its application to balancing a bicycle, this mechanical

system corresponds to the rider's body plus his bicycle. In other applications, the mechanical system may also involve objects in the environment that are sensed from a distance using vision and/or audition. The mechanical system receives input \mathbf{z} from the motor output system (in black), which adds noise \mathbf{m} to the optimal control action \mathbf{u} . The sensory input system (in green) maps the state variables \mathbf{x} onto sensory variables (as specified by the matrix C), adds noise \mathbf{s} and feeds the resulting sensory input \mathbf{y} into the computational system (in blue).

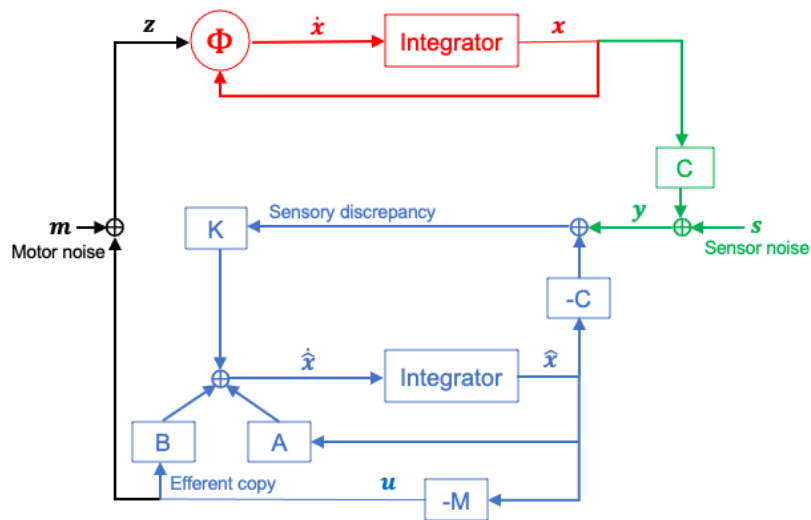


Figure 3: Sensorimotor control of a mechanical system (in red) by input from a computational system (in blue). The mechanical system is governed by the nonlinear differential equations $\dot{\mathbf{x}} = \Omega(\mathbf{x}, \mathbf{z})$, and the computational system produces an optimal control action \mathbf{u} . The motor output system (in black) adds noise \mathbf{m} to \mathbf{u} and feeds this into the mechanical system. The sensory input system (in green) maps the state variables \mathbf{x} to sensory variables, adds noise \mathbf{s} and feeds the resulting sensory input \mathbf{y} into the computational system. The computational system calculates an optimal internal state estimate $\hat{\mathbf{x}}$ by integrating a linear differential equation (characterized by the matrices A , B , C , and the Kalman gain K) that takes the sensory feedback \mathbf{y} as input. The optimal control action \mathbf{u} is obtained from $\hat{\mathbf{x}}$ and the LQR gain $-M$.

The computational system consists of two components: (1) the internal model, which calculates an optimal internal state estimate $\hat{\mathbf{x}}$ by integrating a linear differential equation (characterized by the matrices A , B , C and the Kalman gain

K) that takes the sensory feedback \mathbf{y} as input, and (2) the feedback control law, which determines the control action \mathbf{u} by multiplying the state estimate $\hat{\mathbf{x}}$ with the linear quadratic regulator (LQR) gain $-M$ (minus sign added for consistency with the existing literature). The matrices A , B and C must be learned from experience with the mechanical system. Useful reference values for A and B can be obtained from the first order Taylor approximation of the nonlinear $\Omega(\mathbf{x}, \mathbf{u})$ at the unstable fixed point $\mathbf{x} = \mathbf{0}$ and $\mathbf{u} = \mathbf{0}$. That is, $\Omega(\mathbf{x}, \mathbf{u})$ can be linearly approximated by $A\mathbf{x} + B\mathbf{u}$, with A and B being the Jacobian of $\Phi(\mathbf{x}, \mathbf{u})$ at the unstable fixed point.

Motor and sensor noise

The behavior of the combined system in Figure 3 (including the mechanical, motor output, sensory input, and computational subsystem) is affected by motor and sensor noise. Noise will adversely affect the stabilizing performance of the combined system (i.e., how close \mathbf{x} stays to its target value): motor noise directly feeds into the mechanical system, and sensor noise degrades the internal state estimate.

Our model for the motor input \mathbf{z} to the mechanical system is a simple errors-in-variables model: $\mathbf{z} = \mathbf{u} + \mathbf{m}$. And our model for the sensory input \mathbf{y} to the computational system is the linear model $\mathbf{y} = C\mathbf{x} + \mathbf{s}$. All variables are functions of continuous time. I assume that the noise terms \mathbf{m} and \mathbf{s} are linear combinations of independent vector-valued Wiener processes $\mathbf{v}^{(1)}$ and $\mathbf{v}^{(2)}$:

$$\mathbf{z} = \mathbf{u} + \Phi^{1/2}d\mathbf{v}^{(1)} \quad \text{Eq. 1}$$

$$\mathbf{y} = C\mathbf{x} + \Xi^{1/2}d\mathbf{v}^{(2)} \quad \text{Eq. 2}$$

The scaling matrices $\Phi^{1/2}$ and $\Xi^{1/2}$ determine the covariance of the motor noise $\mathbf{m} = \Phi^{1/2}d\mathbf{v}^{(1)}$ and the sensor noise $\mathbf{s} = \Xi^{1/2}d\mathbf{v}^{(2)}$. Specifically, the motor and the sensor noise are normally distributed with covariance matrices Φdt and Ξdt , respectively.

Stochastic OFC deals with noise in an optimal way

Stochastic OFC provides the tools to deal with motor and sensor noise, and it does so in an optimal way if the noise is Gaussian and additive [16]. This optimality is central to our model for sensorimotor control, which I now formulate with the detail that is required to simulate it on a computer:

1. The CNS learns from experience the following matrices: A , B , C , and the covariances of the motor and the sensor noise. For the purposes of this paper, the matrix C that maps \mathbf{x} onto \mathbf{y} is assumed to be known. The learned noise covariance matrices can be given plausible values, as I will describe in the Results section.
2. The control actions are produced by an internal model that is based on the following linear approximation of the other three systems:

$$\dot{\mathbf{x}} = A\mathbf{x} + B\mathbf{u} + \Sigma^{1/2}d\mathbf{w}^{(1)} \quad \text{Eq. 3}$$

$$\mathbf{y} = C\mathbf{x} + \Psi^{1/2}d\mathbf{w}^{(2)} \quad \text{Eq. 4}$$

in which $\mathbf{w}^{(1)}$ and $\mathbf{w}^{(2)}$ are independent vector-valued Wiener processes. The terms $\Sigma^{1/2}d\mathbf{w}^{(1)}$ and $\Psi^{1/2}d\mathbf{w}^{(2)}$ are simulated versions of the motor and sensor noise. These noise terms are normally distributed with covariance matrices Σdt and Ψdt , respectively. The matrix Σ represents the learned amplitude of the movement inaccuracies that are produced by a noisy motor input ($\mathbf{u} + \text{noise}$), and the matrix Ψ represents the learned amplitude of the sensory discrepancies ($\mathbf{y} - C\mathbf{x}$). Although the actual and the simulated state may differ, I will use the same state variable \mathbf{x} for the mechanical model $\dot{\mathbf{x}} = \Omega(\mathbf{x}, \mathbf{z})$ as for the linear model in Eq. 3 and Eq. 4. The representation of this linear model in Eq. 3 and Eq. 4. is called a state-space representation.

3. The CNS calculates the control action \mathbf{u} such that a cost functional J is minimized:

$$J = \lim_{T \rightarrow \infty} \frac{1}{T} \mathcal{E} \left(\int_0^T [\mathbf{x}(t)' Q \mathbf{x}(t) + \mathbf{u}(t)' R \mathbf{u}(t)] dt \right) \quad \text{Eq. 5}$$

in which $\mathcal{E}(\cdot)$ denotes expected value, and Q and R are positive definite matrices of the appropriate dimensions. The component $\mathbf{x}(t)' Q \mathbf{x}(t)$ quantifies the precision of the internal state variable \mathbf{x} when the target state

equals $\mathbf{0}$; for the general case of a target state equal to \mathbf{c} , this component is $[\mathbf{x}(t) - \mathbf{c}]'Q[\mathbf{x}(t) - \mathbf{c}]$. The component $\mathbf{u}(t)'R\mathbf{u}(t)$ quantifies the energetic cost.

4. Under the linear model in Eq. 3 and Eq. 4., the cost functional J is minimized by control action $\mathbf{u} = -M\hat{\mathbf{x}}$, in which $-M$ is the LQR gain, and $\hat{\mathbf{x}}$ is an optimal state estimate defined by this ODE:

$$\dot{\hat{\mathbf{x}}} = (A - BM)\hat{\mathbf{x}} + K(\mathbf{y} - C\hat{\mathbf{x}}) \quad \text{Eq. 6}$$

The term $(A - BM)\hat{\mathbf{x}} = A\hat{\mathbf{x}} + B\mathbf{u}$ only depends on the internal model, and the term $K(\mathbf{y} - C\hat{\mathbf{x}})$ also depends on the sensory feedback \mathbf{y} . The matrix K is the Kalman gain, which depends on A , C , Σ , and Ψ , the covariance matrices of the learned motor and sensor noise. The LQR gain $-M$ depends on the matrices A , B , Q , and R .

Motor and sensor noise have both a direct and an indirect effect on the stabilizing performance of the combined system: (1) motor and sensor noise directly feed into, respectively, the mechanical and the computational system, and (2) via the Kalman gain K , the state estimate $\hat{\mathbf{x}}$ depends on the internal covariance matrices Σ and Ψ , which the CNS learns from experience with the actual motor and sensor noise.

Is the optimal model good enough?

For stochastic OFC to be a good model for bicycle balance control, the bicycle and the rider must remain balanced over a range of lean and steering angles that is observed in reality. Importantly, the optimality of stochastic OFC does not automatically ensure that the model is also good enough in that respect [25]. The quality of the model depends on how well the linear internal model approximates the external nonlinear dynamical system plus the motor and the sensor noise covariance matrices. The accuracy of the approximation in turn depends on two factors: (1) how good is the linear approximation with optimal values for the linear model's parameters A , B , C , Σ and Ψ , and (2) how close are the actual values to these optimal parameter values? The quality of the optimal linear approximation is investigated in the first of three simulation studies. Specifically,

in this simulation study, I will evaluate whether stochastic OFC with optimal parameter values can balance the model bicycle for steering and lean angles that are observed with real riders on real bicycles, without requiring steering angular rates that no real rider can produce. However, it is unlikely that the linear model's parameters are exactly at their optimal values, and the possible consequences of this are discussed next.

Which learned parameters are responsible for stabilization failures?

Under the model, there are two factors that contribute to stabilization failures (i.e., bicycle and rider falling over): (1) motor and sensor noise, and (2) the control mechanism. In this paper, I will focus on the role of the control mechanism; the motor and the sensor noise will be given realistic values (see *Is the optimal model good enough to balance a bicycle under realistic conditions?*).

The control mechanism is fully specified by (1) the matrices A , B , and C of the state-space representation, and the Kalman gain K , which together determine the state estimate $\hat{\mathbf{x}}$, and (2) the LQR gain $-M$, which determines the control action $\mathbf{u} = -M\hat{\mathbf{x}}$. The Kalman gain is a function of the matrices A , B , C , Σ and Ψ , and the LQR gain is a function of A , B , Q , and R . Because C is assumed to be known, and Q and R determine the tradeoff between precision and energy expenditure, I will focus on A , B , Σ and Ψ . The CNS must learn these parameters from experience with the mechanical system and the motor and sensor noise.

It is very likely that the CNS has learned a sub-optimal approximation of the mechanical system, and this would be reflected in matrices A and B that are worse than those obtained as the Jacobian of $\Omega(\mathbf{x}, \mathbf{u})$ at the unstable fixed point. If the stabilization performance would quickly decrease with the difference between the actually learned and the optimal matrices A and B , this would argue against stochastic OFC as a good model for bicycle balance control. In fact, the lower the robustness against differences between the learned and the optimal matrices A and B , the smaller the margin of error for the learning ability of the CNS.

The same reasoning applies to the learned noise covariance matrices Σdt and Ψdt : the more accurate the learned covariance matrices, the smaller the adverse effect of the noise on the stabilizing performance. This fact can be proved for a linear mechanical system, and it is approximately true for a nonlinear mechanical system in a region of the state-space for which this system is approximately linear. Specifically, for a linear mechanical system, $\Phi(\mathbf{x}, \mathbf{z}) = A\mathbf{x} + B\mathbf{z}$, and using Eq. 1, this can be rewritten as $\Phi(\mathbf{x}, \mathbf{z}) = A\mathbf{x} + B\mathbf{u} + B\Phi^{1/2}d\mathbf{v}^{(1)}$. Comparing this with the first state-space equation of the computational system (Eq. 3), we see that the two systems are identical if $\Sigma = B\Phi B^T$. In addition, comparing Eq. 2 and Eq. 4, we see that the sensory system is identical to the state-space equation of the computational system if $\Psi = \Xi$. Thus, optimal control of a linear mechanical system involves a Kalman gain that is calculated using $\Sigma = B\Phi B^T$ and $\Psi = \Xi$.

In the same way as for the learned matrices A and B , if the stabilization performance would quickly decrease with the difference between the actual and the optimal Σ (Ψ), this would argue against stochastic OFC as a good model for bicycle balance control. In fact, this would imply a small margin of error for the learning ability of the CNS.

How plausible is stochastic OFC as a model for sensorimotor control?

To evaluate the plausibility of stochastic OFC as a model for sensorimotor control, in three simulation studies, I address the following questions: (1) Is the optimal model good enough to balance a bicycle under realistic conditions, and (2) Is the model robust against variations in the parameter values that the CNS must learn? I begin by describing what is meant by “realistic conditions”.

What are realistic steering angles, lean angles, and steering angular rates?

For our model to be plausible, it must be able to balance the SDP for steering and lean angles that approach the values observed with real riders on real bicycles,

without requiring steering angular rates that no real rider can produce. To find realistic steering and lean angles, consider a rider that makes a steady U-turn at $v = 4.3056$ m/s (=15.5 km/h) on one of the narrowest two-way roads in the Netherlands (4.5 m.). The steering angle that is needed to keep a steady-state turn with radius $R = 4.5$ m. follows from the kinematics of the SDP (see *Methods and Models*). Specifically, for the kinematic model, the following equation holds [26]:

$$\tan(\delta) \cos(\beta) = \frac{W}{R}$$

in which β (the slip angle) is a function of the steering angle δ (see *Methods and Models*). For a wheelbase $W = 1.12$ m. and a radius $R = 4.5$ m., the corresponding steering angle δ is equal to 0.24 rad. To stay balanced in the U-turn, the lean angle of the combined CoG must be such that it exactly compensates for the turn-induced centrifugal acceleration (via the lean-induced gravitational acceleration). This lean angle is obtained as $\sin^{-1}((v^2/R)/g) = \sin^{-1}((4.3056^2/4.5)/9.81) = 0.4344$. Because the model wants to keep the bicycle upright (instead of keeping it in a steady U-turn), the lean angle of the combined CoG should be less than 0.4344, and the steering angle should be more than 0.24 rad.

The model's steering input should also result in steering angular rates that a real rider can produce. To find an upper limit to the steering angular rate, I start from the fastest hand movement observed in a reaching task: 4 m/s [27]. Combining this linear velocity with a typical commuter handlebar width of 0.7 m, I find a critical steering angular rate of 11.45 rad/s.

Is the optimal model good enough to balance a bicycle under realistic conditions?

To evaluate the plausibility of the model, I simulated state variables for increasing noise amplitudes. Noise enters the combined system via the motor output \mathbf{z} and the sensory input \mathbf{y} and its amplitude is determined by the motor and the sensor noise covariance matrices Φ and Ξ . The dimensions of Φ correspond to the two control actions, steering and upper body lean torque ($\mathbf{u} = [T_\delta, T_{\phi_2}]^T$), and the dimensions of Ψ correspond to the six sensory inputs. In my simulations, I

independently varied the amplitudes of three different noise types: steering noise, upper body noise, and sensor noise. I did this by specifying Φ and Ψ as diagonal matrices defined by three scalar constants, c_δ , c_{ϕ_2} and c_y : $\Phi = \text{diag}([c_\delta, c_{\phi_2}])$, and $\Psi = \text{diag}([c_y, c_y, c_y, c_y, c_y, c_y])$. There were only small differences between the three noise types with respect to how much they affected the lean and the steering angles. These differences did not justify a discussion of the more complicated pattern of results as compared to the results for homogeneous noise amplitudes, $c_\delta = c_{\phi_2} = c_y = c$.

I evaluated the plausibility of the model at its optimal parameter values. Specifically, the matrices A and B were set equal to the Jacobian of the EoM at the unstable fixed point, and the learned motor and sensor noise covariance matrices Σ and Ψ (which co-determine the Kalman gain K) were given values that correspond to the actual motor and sensor noise covariance matrices Φ and Ξ (see *Which learned parameters are responsible for stabilization failures?*).

I calculated the LQR gain for a cost functional that is defined by $Q = \text{diag}([0.01, 1, 0.5, 0.01, 1, 0.5])$ and $R = \text{diag}([1, 1])$. For Q , remember that the state variables are ordered as follows: $\mathbf{x} = [\delta, \phi_1, \phi_2, \dot{\delta}, \dot{\phi}_1, \dot{\phi}_2]^T$. Thus, I have specified Q to reflect that the CNS attaches most weight to the stabilization of the lower body (angle and angular rate), somewhat less weight to the stabilization of the upper body, and almost doesn't care about the steering angle. In an unsystematic way, I also tried other values for Q and R , that differed from the ones above by an order of magnitude. These variations did not have a spectacular effect on the simulations.

I linearly increased the values of the noise amplitude c from 0.01 to 0.20, and simulated the model under the resulting motor and sensor noise. For every noise amplitude, I simulated 100 trials of 60 seconds at $\Delta t = 0.01$. I used the simulated state variables to quantify how well the mechanical system is stabilized. As a quantification, I used the maximum absolute (MaxAbs) value of the state variables and the lean angle at the combined CoG. A plausible model must be able to balance the SDP with MaxAbs values for the lean and steering angles that

approach, respectively, 0.4344 and 0.24 rad., with a MaxAbs value for the steering angular rate that does not exceed 11.45 rad/s. MaxAbs was calculated per trial, and subsequently averaged.

The results of this simulation are shown in Figure 4. As expected, the MaxAbs steering angle, combined CoG lean angle, and steering angular rate all increase with the noise amplitude (see Figure 4 left panel). Shortly after noise amplitude 0.1, there is a sharp increase in the MaxAbs values, and this is due to the fact that, on a subset of the trials, Matlab's ODE solver (ode45) could not reach the required accuracy for the numerical integration; when this happened, the simulation was interrupted. The percentage of interrupted trials increased from 15% to 41% over the noise level range [0.135,0.200].

It is important to establish that the results are not limited by the accuracy requirements of Matlab's ODE solver. For this, it is useful to present our results separately for the completed and the interrupted trials (see Figure 4, right panel). The crucial observation in the right panel of Figure 4 is that, for the interrupted trials, the MaxAbs combined CoG lean angles exceed $\pi/2$, a value that cannot be attained without touching the road surface. The results of our simulation study are thus not limited by the accuracy requirements of Matlab's ODE solver.

I now discuss the results for the completed simulations. At the highest noise amplitude, the maximum absolute steering angle is 0.3795 rad., which produces a sharper turn than the 0.24 rad. that is needed for a steady 4.5 m. U-turn. At the same noise amplitude, the combined CoG lean angle is 0.3635, which is less than the 0.4344 rad. that is required for a steady 4.5 m. U-turn. Thus, the model can make sharper turns than what is needed to exactly compensate for the gravitational force produced by the largest lean angles. Thus, in line with the fact that the model is designed for balancing, it uses steering to bring the bicycle upright. Finally, the model balances the bicycle with a maximum steering angular rate (1.2680 rad./s.) that is much less than the rate that corresponds to the fastest hand movement observed in a reaching task (11.45 rad./s.). Thus, the model can balance the bicycle under realistic conditions.

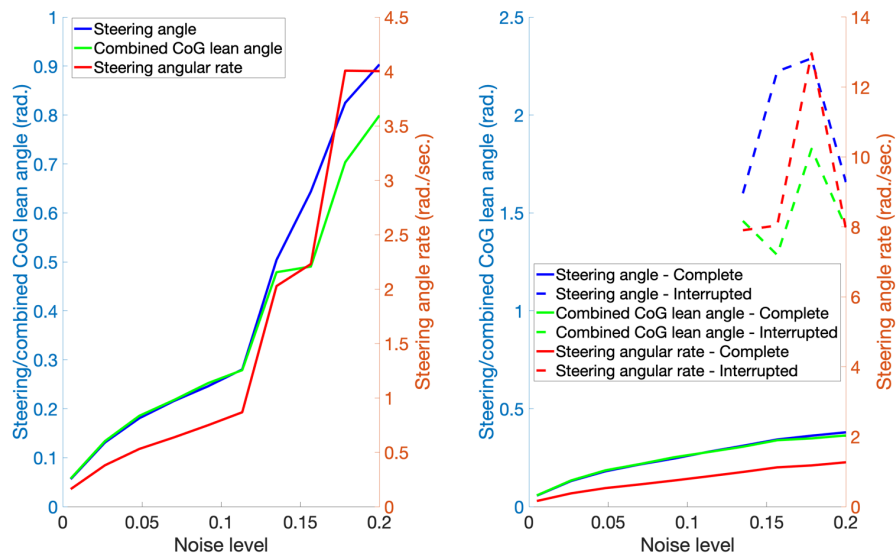


Figure 4: Maximum absolute (MaxAbs) steering angle, combined CoG lean angle, and steering angular rate as a function of the noise level in the simulation. In the left panel, I show the average MaxAbs over all simulated trials, and in the right panel I show the average MaxAbs averaged separately over the completed and interrupted trials. In this simulation, the Kalman and the LQR gain were calculated at the optimal learned parameter values (see text).

Is the model robust against variations in the parameter values that the CNS must learn?

The CNS must learn the internal model from experience with the rider's body plus bicycle. This learning process takes time, and therefore the model must be robust against variations in the values of its parameters. I investigated this robustness in two simulation studies in which I manipulated the accuracy of (1) the learned noise covariance matrices Σ and Ψ , and (2) the learned system (state) matrix A . The learned noise covariance matrices and the learned system matrix correspond to two different aspects of the environment that the CNS must learn: (1) the reliability of the motor output and the sensory input, and (2) the physical laws that govern the movements of our body and bicycle. They also play different roles in the computational model: the learned noise covariance matrices only affect the Kalman gain (which updates the internal state estimate), whereas the learned

system matrix also affects the LQR gain (which maps the state estimate on the control action).

In the first simulation study, I investigated the robustness against variations in the learned noise covariance matrices Σ and Ψ , and did this by systematically varying the difference between the learned noise covariance matrices Σ and Ψ , and the corresponding optimal values $\Sigma = B\Phi B^T$, $\Psi = \Xi$. I ran the study with actual motor and sensor noise covariance matrices $\Phi = \text{diag}([c_\delta, c_{\phi_2}])$ and $\Xi = \text{diag}([c_y, c_y, c_y, c_y, c_y, c_y])$, in which I set $c_\delta = c_{\phi_2} = c_y = 0.11$. I manipulated the accuracy of Σ and Ψ by means of a noise fraction f with logarithmically spaced values between 0.1 and 10. I investigated two types of inaccuracy: motor noise inaccuracy ($\Sigma = fB\Phi B^T$) and sensor noise inaccuracy ($\Psi = f\Xi$).

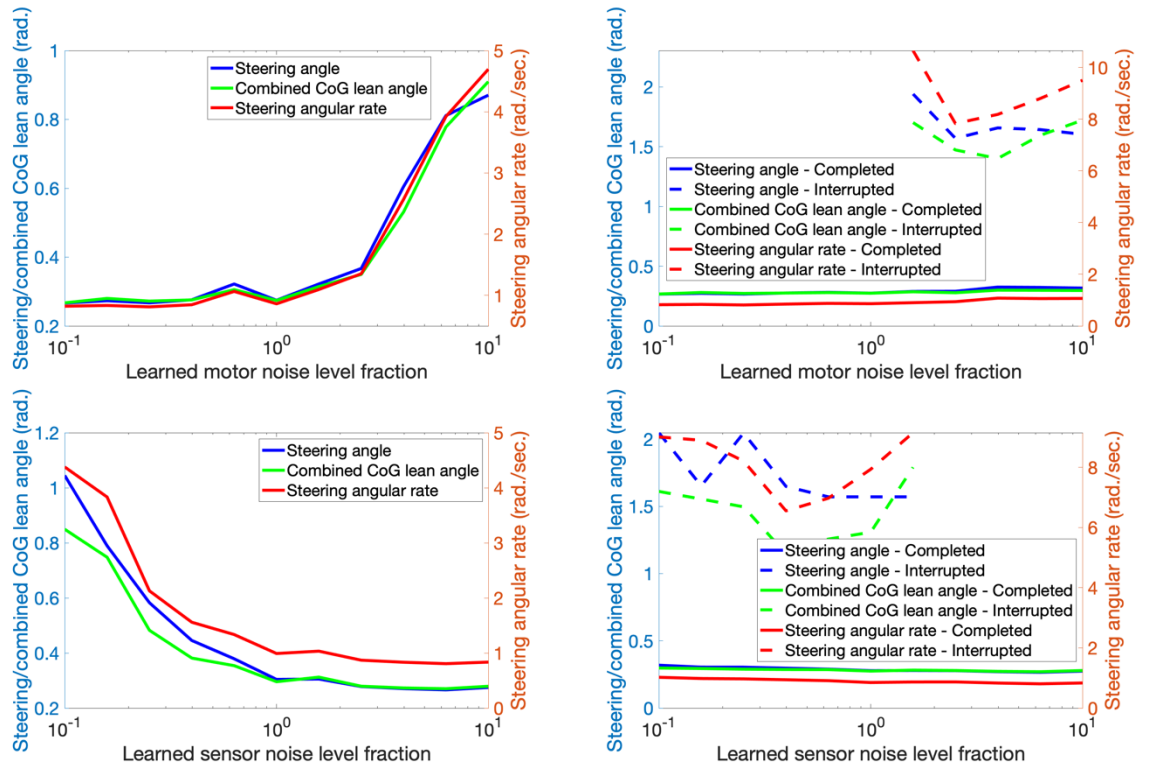


Figure 5: Maximum absolute (MaxAbs) steering angle, combined CoG lean angle, and steering angular rate as a function of the learned motor (top row) and the learned sensor noise level fraction (bottom row). Across all simulations, the actual noise amplitude was kept constant; only the learned noise covariance matrices were manipulated. Both the learned motor noise (top row) and the learned sensor noise (bottom row) were set equal to a fraction of the actual noise amplitude, with

the fraction ranging from 0.1 to 10, and logarithmically spaced. In the left panels, I show the average MaxAbs over all simulated trials, and in the right panels I show the average MaxAbs averaged separately over the completed and the interrupted trials.

The results are shown in Figure 5, separately for the motor (top row) and the sensor noise inaccuracy (bottom row). The main pattern is that, when the learned motor noise covariance matrix is manipulated, MaxAbs increases with the noise fraction for all three angular variables, whereas it decreases when the learned sensor noise covariance matrix is manipulated. Inspecting MaxAbs for all trials (the two left plots), one sees a clear elbow at the point where the noise fraction equals one (the most accurate learned noise covariance matrix). As is clear from the two plots on the right, this is due to the fact that before (for the learned motor noise) or after (for the learned sensor noise) this point, on a subset of the trials, Matlab's ODE solver could not reach the required accuracy for the numerical integration. The largest percentage of interrupted trials for the learned motor noise manipulation was 57% (for noise fraction 0.1), and for the learned sensor noise manipulation this was 58% (for noise fraction 10). Thus, our model has a specific type of robustness against inaccuracies in the learned noise covariance matrices: the stabilization is robust against learned motor noise covariances that are too small and learned sensor noise covariances that are too large.

At first sight, these results seem consistent with a scenario in which the stabilization improves as the control actions are more based on the internal model's estimate of the current state (i.e., the term $(A - BM)\hat{\mathbf{x}}$ on the right-hand side of Eq. 6) as compared to the sensory discrepancies (i.e., the term $(\mathbf{y} - C\hat{\mathbf{x}})$ on the right-hand side of Eq. 6). The relative weighting of these two sources of information is controlled by the Kalman gain K , which determines the contribution of the sensory discrepancy to the state estimate. However, inspection of the Kalman gains for the different noise level fractions revealed that this scenario cannot explain the results: although the Kalman gain matrices changed over the noise level fractions, there was no overall increase or decrease. This is clear from Figure 6, which shows a color image of the ratio of the Kalman gain matrices for the largest and the smallest learned motor noise level fraction. In case of an overall increase, for all cells, the ratios should be positive and larger

than 1, which is not the case. A similar image was obtained when contrasting the Kalman gain matrices for the largest and the smallest learned sensor noise level fraction.

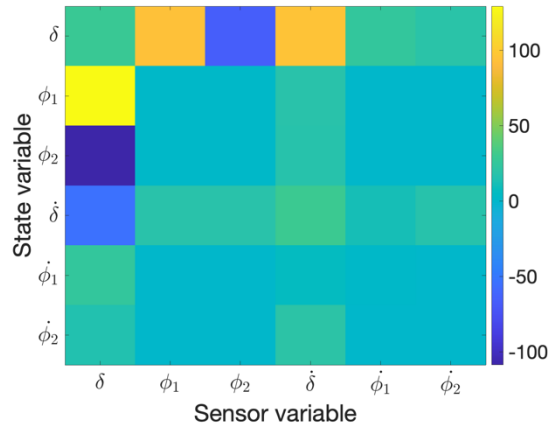


Figure 6: Element-wise ratio of the Kalman gain matrices for the largest and the smallest learned motor noise level fraction (noise level fraction 10 over 0.1). The tick labels for the state and the sensor variable are identical because the defining matrix for the sensory system (C) is the identity matrix.

In sum, the model is robust against variations over a range of values for the learned motor and sensor noise covariances. This robustness is due to the ability of the Kalman gain to differentially weigh the contribution of the different elements of the sensory discrepancy vector to the state estimate.

In the second simulation study, I systematically varied the difference between the learned system matrix A and the optimal system matrix obtained as the Jacobian of $\Omega(\mathbf{x}, \mathbf{u})$ with respect to \mathbf{x} and evaluated at the unstable fixed point. In doing this, I made use of the fact that the optimal system matrix depends on the bicycle speed (because $\Omega(\mathbf{x}, \mathbf{u})$ depends on the centrifugal acceleration; see Eq. 7 and 9). In fact, I investigated the robustness of the model against inaccuracies in A that result from misestimation of the bicycle speed. I simulated an SDP with an actual speed of $v = 4.3$ m/sec., and for manipulating the learned system matrix A , I used the dependence of the EoM on the bicycle speed v . I calculated 13 different inaccurate system matrices A by calculating the Jacobian of $\Omega(\mathbf{x}, \mathbf{u})$ for linearly spaced values of v between 85 and 115 percent of the actual speed.

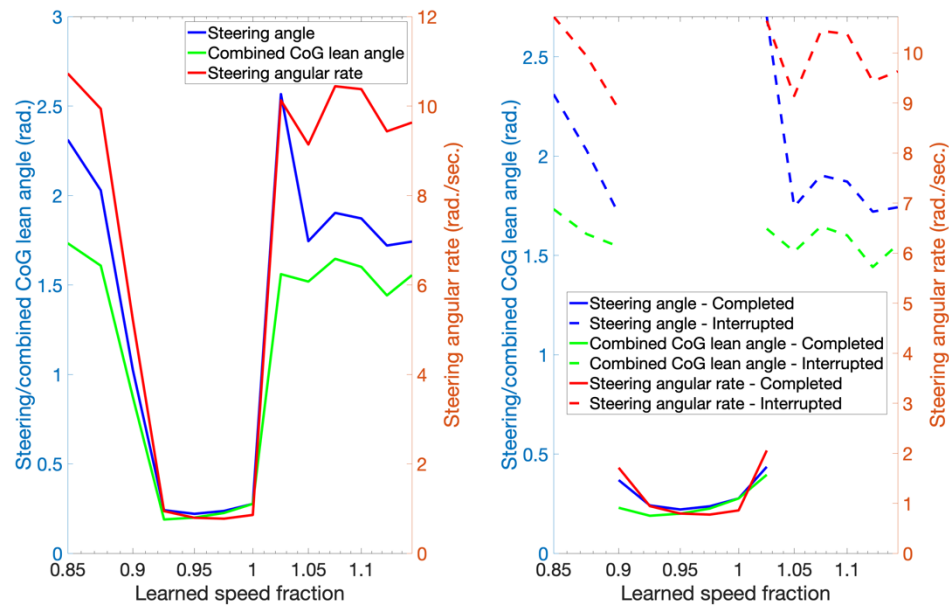


Figure 7: Maximum absolute (MaxAbs) steering angle, combined CoG lean angle, and steering angular rate as a function of the learned speed fraction. Across all simulations, the actual speed was kept constant; only the learned speed and the associated system matrix was manipulated. The learned speed was set equal to a fraction of between 0.85 and 1.15 of the actual speed. In the left panel, I show the MaxAbs averaged over all simulated trials, and in the right panel the MaxAbs averaged separately over the completed and the interrupted trials.

From the results in Figure 7 it is clear that stabilization strongly depends on the accuracy of the learned speed: completed trials were only found for learned speed fractions between 0.9 (51% completed) and 1.025 (5% completed). The robustness is asymmetrical around the true speed: there is a small range of underestimated speeds (fractions 0.9 to 1) that still allow for stabilization, but for overestimated speeds this range is much smaller. Thus, the model is not robust against inaccuracies in A that result from misestimation of the bicycle speed.

Discussion

I proposed and evaluated a model for bicycle balance control. The central concept in this model is a computational system, implemented in the CNS, that not only controls but also learns a mechanical system that exists outside the CNS. At the interface between these two systems, there is a motor output system that transfers a control signal to the mechanical system, and a sensory system that maps the state of the mechanical system into the computational system. The computational system can simulate the combined mechanical, motor output, and sensory input system. It does so by means of a learned approximation of (1) the physical laws that govern the mechanical system, (2) the mapping performed by the sensory system, and (3) the reliability of the motor output and the sensory input. In my implementation of the computational system, I assumed that (1) the optimal learned approximation of the physical laws is linear, with the defining matrices for the mechanical system (A and B) being the Jacobian of the EoM evaluated at the unstable fixed point, and (2) the optimal learned approximation of the reliability are the noise covariance matrices of the optimal linear approximation of the combined mechanical, motor output, and sensory input system.

The control of the mechanical by the computational system is optimal in the sense of stochastic OFC. It then follows that the stabilization performance of the model only depends on three factors: (1) the amplitude of the motor output and the sensory input noise, (2) the optimality criterion (i.e., the expected cost-to-go), and (3) the accuracy of the learned approximation. Of these three, the accuracy of the learned approximation is the most interesting from a cognitive point of view, and the amplitude of the motor output and the sensory input noise is the most interesting from a physiological point of view.

I have applied this model to the balancing of a bicycle. This is uncommon in sensorimotor control, in which the relevant data are often collected in experimental paradigms that ask for more isolated movements (e.g., reaching, pointing, lifting) that naturally occur as a part of more complex movements involving the whole body. From this perspective, balancing a bicycle is more like walking on a treadmill with the additional advantage that the movements are

strongly constrained by the geometry of the bicycle and the rider's position on it. Therefore, balancing a bicycle has become a topic of interest for non-academics, of which some contribute valuable observations by experimenting with the handling properties of a bicycle (e.g., by reversing the steering response).

I conducted three simulation studies. In the first of these studies, I demonstrated that the model is able to balance a bicycle under realistic conditions. In the second study, I demonstrated that the model's stabilization performance is robust against inaccuracies in the learned noise covariance matrices: the stabilization performance is robust against learned motor noise covariances that are too small and learned sensor noise covariances that are too large. Finally, in the third study, I demonstrated that the model is not robust to variations in the learned system matrix caused by a misestimation of the speed.

As holds for every model, our model is only an approximation of reality. It is important to be aware of a few aspects for which I made a choice for the sake of computational feasibility or simplicity. Not all choices are inevitable, but more work is needed to extend the model, allowing it to perform more sophisticated computations. The first useful extension immediately follows from the third simulation study: if the model must apply to a wide range of speeds, a mechanism must be added for accurate speed estimation and selection of the appropriate system matrix. One likely source of speed information is optic flow, and this suggests that the sensory feedback should not only contain information about the rider's body (i.e., its joint angles), but also about the rider's position in the environment, as sensed from a distance using vision. However, many experienced cyclists can also ride on stationary bicycle rollers, and this suggest that optic flow is not the only possible source of speed estimation.

The second aspect to be aware of, is that the computational system is based on a linear approximation of the unknown mechanical system. Although it is difficult to argue against the idea that the internal model must be based on some sort of approximation, there is no reason that it should be linear and optimal for a single point (i.e., the unstable fixed point). For example, if it were the optimal linear approximation for the unstable fixed point, and the bicycle rider had learned the

linear coefficients on the basis of experience with lean angles below 5 degrees, then this linear approximation would also allow him to simulate the linear ODE in Eq. 3 for much larger lean angles than he is familiar with. This would allow him to balance his bicycle outside the range he is familiar with. Whether this is actually possible, is still an empirical question.

The third aspect to be aware of pertains to the biological delays between the state estimate $\hat{\mathbf{x}}$ and (1) the mechanical system input \mathbf{z} (the motor delay), and (2) the sensory feedback \mathbf{y} (the sensory delay). The motor delay is caused by the fact that the control action must pass via motor axons and muscles before it affects the mechanical system, and the sensory delay is caused by the fact that the sensory feedback has to pass via a series of sensory neurons before it arrives in the computational system. In our model, I assumed both delays to be zero, which is unrealistic. With respect to the motor delay, for a model that only estimates the current state $\hat{\mathbf{x}}(t)$, the following must hold:

$$\mathbf{z}(t + T_{mot}) = -M\hat{\mathbf{x}}(t) + \mathbf{m}(t + T_{mot}) \quad ,$$

in which T_{mot} is the motor delay. Even for a small motor noise \mathbf{m} and a state estimate $\hat{\mathbf{x}}$ that approximates the mechanical system states \mathbf{x} very well, the torque $\mathbf{z}(t + T_{mot})$ will not stabilize the mechanical system if $\mathbf{x}(t + T_{mot})$ differs too much from $\mathbf{x}(t)$. This is a well-known problem in sensorimotor control, and it has been proposed that the prediction of future states may solve it [28-33]. This implies that the estimate $\hat{\mathbf{x}}(t)$ is replaced by a prediction $\tilde{\mathbf{x}}(t, T_{mot})$, which extrapolates the estimate at time t (i.e., $\hat{\mathbf{x}}(t)$) to time $t + T_{mot}$.

With respect to the sensory delay, for a model that only estimates the current state $\hat{\mathbf{x}}(t)$, the following must hold:

$$\dot{\hat{\mathbf{x}}}(t) = (A - BM)\hat{\mathbf{x}}(t) + K[\mathbf{y}(t - T_{sens}) - C\hat{\mathbf{x}}(t)] \quad ,$$

in which T_{sens} is the sensory delay. Similar to the problem caused by a motor delay, if $\mathbf{x}(t - T_{sens})$ (the state reflected by $\mathbf{y}(t - T_{sens})$) differs too much from $\mathbf{x}(t)$, the state estimate $\hat{\mathbf{x}}(t)$ will be incorrectly updated. This problem can be solved by only updating the past state estimate $\hat{\mathbf{x}}(t - T_{sens})$. Combining this solution with the one for the motor delay, this results in a model in which the state estimate $\hat{\mathbf{x}}$ lags $T_{mot} + T_{sens}$ behind the true state \mathbf{x} , and the control action is calculated using the prediction $\tilde{\mathbf{x}}(t, T_{mot} + T_{sens})$. More work is required to

evaluate whether the SDP can be balanced with a realistic motor and sensory delay, and whether prediction is necessary to achieve this.

The fourth aspect of the model to be aware of is that the control action is specified in torque values, whereas the output of the CNS are neuronal firing rates which are converted to joint torques by the muscles. This firing-rate-to-torque conversion is not a part of the model, and this most likely has consequences for the model's validity. For instance, in the computational model, the LQR gain performs a linear mapping from the state estimate to the control action, and this ignores the fact that the muscles may not be able to produce the required torques. This is especially important in the context of ageing and physical training, which affect the available torque ranges. Most likely, motor skill learning involves two parallel processes, one at the muscular level that determines the available torque ranges, and one at the level of the CNS that learns the mapping from the state estimate to the required torques. For the model to be valid, the CNS-level process must be informed by the available torque ranges.

It is possible to extend the model such that it incorporates the firing-rate-to-torque conversion, and this requires knowledge of the muscular physiology. Specifically, if the optimal control action \mathbf{u} is a vector of firing rates, then one needs a new matrix B that must be decomposable as follows:

$$B = B_{\dot{\mathbf{x}} \leftarrow \mathbf{u}} = B_{\dot{\mathbf{x}} \leftarrow \boldsymbol{\tau}} B_{\boldsymbol{\tau} \leftarrow \mathbf{u}} \quad ,$$

in which $B_{\boldsymbol{\tau} \leftarrow \mathbf{u}}$ specifies the mapping from the firing rate vector \mathbf{u} on the joint torques $\boldsymbol{\tau}$, and $B_{\dot{\mathbf{x}} \leftarrow \boldsymbol{\tau}}$ (the old matrix B) specifies the mapping from the joint torques on the state derivatives $\dot{\mathbf{x}}$. The matrix $B_{\boldsymbol{\tau} \leftarrow \mathbf{u}}$ must be specified on the basis of knowledge of muscular physiology, and the matrix $B_{\dot{\mathbf{x}} \leftarrow \boldsymbol{\tau}}$ can be calculated as the Jacobian of $\Omega(\mathbf{x}, \boldsymbol{\tau})$ with respect to $\boldsymbol{\tau}$, evaluated at $\boldsymbol{\tau} = \mathbf{0}$.

The fifth aspect to be aware of is that the control actions are only two-dimensional (steering and hip torque), whereas the number of balance-relevant muscles and joints is much larger. This simplification can be motivated by the fact that the relevant control input is strongly constrained by the geometry of the bicycle and the rider's position on it. This simplification is specific to balancing a bicycle, and this points to the challenges one may encounter when extending the model to

other forms of balancing (e.g., cycling while standing on the pedals, walking, running, skating, skiing). In principle, the extension is straightforward, as it only requires the EoM for this other form of balancing. However, the challenging part may be the derivation of the EoM, which starts by identifying the balance-relevant joints and selecting the ones that can be actuated. Once the EoM are derived, the linearization and the calculations for the computational system are identical to those for balancing the SDP.

The sixth aspect to be aware of is that the current sensory model is underspecified: it assumes that the sensory input is identical to the state variables \mathbf{x} (as implemented by the assumption that the matrix C equals the identity matrix) plus some noise. From sensory neurophysiology, it is known that information about the state variables (steering, lower body, and upper body angles and angular rates) must be obtained from the proprioceptive and/or the vestibular system, but the details of that knowledge are not yet incorporated in the model.

The seventh aspect to be aware of pertains to the assumption that the motor and the sensor noise are additive, although there is good evidence that motor noise is multiplicative [34, 35]. The advantage of additive over multiplicative noise, is that it is much easier to derive the optimal control actions. For multiplicative noise, optimal control actions were derived by Todorov and colleagues [2, 11], but these are restricted to movements with a finite horizon (e.g., pointing, reaching, throwing, hitting). Keeping balance is an infinite horizon problem (i.e., the cost-to-go functional is an integral from zero to infinity), and this requires mathematical results for which a convenient computational implementation is not yet available [36, 37].

The eight and last aspect to be aware of is that I used a bicycle model without self-stabilizing forces in the front frame. This choice was motivated by my interest in the rider-generated stabilizing forces, but it has the disadvantage that our simulations likely present an unrealistically negative picture of how difficult it is to balance a bicycle. Fortunately, it is straightforward to extend our bicycle model with these self-stabilizing forces, provided one knows how they depend on the state variables.

Concluding, I have proposed and evaluated a model for sensorimotor control that is based on the idea that a computational system in the CNS learns and controls an external mechanical system. This control is optimal in the sense of stochastic OFC. The model can balance a bicycle and its rider under realistic conditions, and is robust against some (but not all) variations in the learned noise covariance matrices. It is not robust to inaccuracies in the learned system matrix caused by a misestimation of the speed. The model is a very useful starting point for investigations into human balance control, and there are several ways in which it can be extended to provide a more realistic account.

Methods and models

The equations of motion (EoM) for the steered double pendulum (SDP)

The SDP is depicted schematically in Figure 8. The SDP contains ingredients of three familiar models: the double compound pendulum on a cart [DCPC, 8], the Acrobot [9], and the torsional spring-mass-damper system. Roughly speaking, the SDP is a double compound pendulum of which the base can be steered by a wheel (instead of a cart) and the joint between the two rods (at the hips) can be actuated, as in the Acrobot. Both actuated joints, one at the handlebars and one at the hips, are modeled as a torsional spring-mass-damper system. I will denote the lower and the upper rod as, respectively, the lower and the upper body. The lower body represents the rear frame plus the rider's lower body; the upper body only represents the rider's upper body.

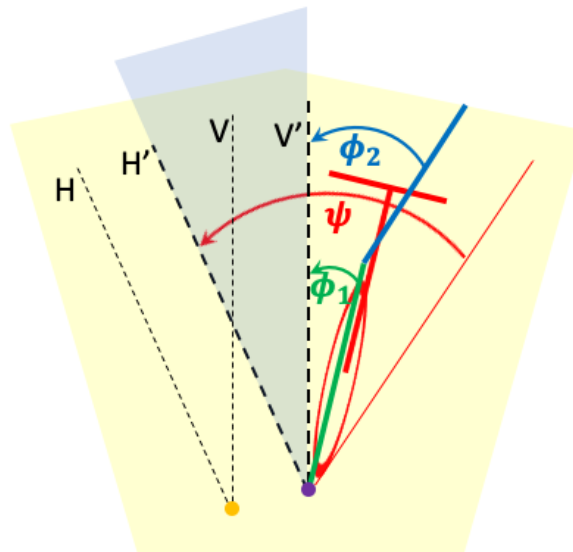


Figure 8: The relevant kinematic variables of the SPD in both an inertial (yellow origin) and a rider/bicycle-centered (purple origin) reference frame. The inertial reference frame has an arbitrary origin, and the rider/bicycle-centered reference frame has its origin at the orthogonal projection of the combined CoM on the LoS. These reference frames have parallel coordinate axes. In green and blue, I depict the lean angles of the lower and the upper body (ϕ_1 and ϕ_2), and in red, I depict the yaw angle ψ of the LoS. The horizontal plane (road surface) is colored light yellow.

The kinematic model

Figure 8 depicts the relevant kinematic variables in both an inertial (yellow origin) and a rider/bicycle-centered (purple origin) reference frame. The inertial reference frame has an arbitrary origin, a vertical coordinate axis V perpendicular to gravity, and an arbitrary horizontal coordinate axis H perpendicular to V . The rider/bicycle-centered reference frame has its origin at the orthogonal projection of the combined CoM on the LoS, and a vertical and horizontal coordinate axis V' and H' that are parallel to those of the inertial reference frame. The rider/bicycle-centered reference frame is non-inertial because, when the bicycle turns, the origin no longer moves in a straight line, and therefore accelerates in the inertial reference frame.

I will use the rider/bicycle-centered reference frame to define three kinematic variables. The first two kinematic variables are the lower and the upper body lean angles (ϕ_1 and ϕ_2), which are defined relative to the vertical axis V' . The third kinematic variable is the yaw angle ψ of the LoS, which is defined relative to the horizontal axis V' . When describing the dynamics of the SDP, we need an expression for the centrifugal acceleration α at the combined CoG. I assume identical speeds at the separate CoGs of the lower and the upper body as well as identical angular rates of the projections on the horizontal plane. Then, the centrifugal acceleration only depends on the yaw angular rate $\dot{\psi} = \partial\psi/\partial t$ and the speed v :

$$\alpha = v\dot{\psi}$$

Crucially, $\dot{\psi}$ depends on the steering angle δ , and this allows the rider to control the LoS.

For the SDP EoM, one must know the precise dependence of $\dot{\psi}$ on δ . Deriving this dependence is a well-known problem in vehicle dynamics [26], and here I use the known result. This result involves the so-called slip angle β , which is the angle between the velocity vector of the combined CoG and the LoS. This slip angle can be obtained as follows:

$$\beta = \tan^{-1} \left(\frac{w_r \tan(\delta)}{W} \right)$$

In this equation, W is the wheelbase and w_r is the position of the combined CoG on the LoS. More precisely, w_r is the distance between the road contact point of the rear wheel and the orthogonal projection of the combined CoG on the LoS. For realistic values ($W = 1.12$, $w_r = 0.291$, $-20^\circ < \delta < 20^\circ$), the slip angle β is almost a linear function of δ :

$$\beta \approx \frac{w_r \delta}{W}$$

For steering angles $-20^\circ < \delta < 20^\circ$, all deviations from linearity are less than 0.36%. I will continue to use this approximation. Following [26], one can obtain the centrifugal acceleration $\alpha(\delta)$ as follows:

$$\alpha(\delta) = v^2 \frac{\cos(\beta)}{W} \tan(\delta) \quad \text{Eq. 7}$$

Note that the centrifugal acceleration is a function of only a single variable, the steering angle δ . This motivates our functional notation $\alpha(\delta)$.

The steering model

The steering model assumes that the steering angle δ is fully controlled by rider-applied forces on the handlebars. Thus, I ignore all forces that may contribute to the bicycle's self-stability.

The steering assembly consists of the front wheel, the fork, the handlebars, and the rider's arms. I model this assembly as a torsional spring-mass-damper system:

$$I_{steer} \ddot{\delta} + C_{steer} \dot{\delta} + K_{steer} \delta = T_\delta \quad \text{Eq. 8}$$

In Eq. 8, I_{steer} is the assembly's rotational inertia, C_{steer} its damping, and K_{steer} its stiffness. The input to the steering assembly is the net torque produced by the rider's muscles, and denoted by T_δ on the right-hand side of Eq. 8.

The double compound pendulum with a steer-actuated base

I model the lean angles ϕ_1 and ϕ_2 as the result of a double compound pendulum on a virtual (zero mass) cart with acceleration equal to $\alpha(\delta)$, the centrifugal

acceleration derived under our kinematic model (see Eq. 7). Like the Acrobot, this double compound pendulum has an actuated joint between the upper and the lower body (the hips). To make our model biologically realistic, I add stiffness and damping to the hips.

The EoM for ϕ_1 and ϕ_2 are obtained by first applying the Euler-Lagrange method to the DCPC with a zero-mass cart, and then adding the constraint that the cart is controlled by the steering-induced centrifugal acceleration $\alpha(\delta)$. The derivation of the DCPC EoM using the Euler-Lagrange method can be found in the literature. Here, I started from Bogdanov (8) and added stiffness, damping and torque input at the joint between the two rods (the hips). Next, I added a constraint that follows from the fact that the bicycle's wheels are oriented perpendicular to the cart's wheels. Specifically, under this constraint, the angles ϕ_1 and ϕ_2 have no direct effect on the position of the base of the first rod (in the DCPC, the point where the cart is attached). Instead, this position is fully controlled by the steering-induced centrifugal acceleration $\alpha(\delta)$. The result is the following:

$$\begin{aligned} & \begin{bmatrix} d_1 \cos(\phi_1) \\ d_2 \cos(\phi_2) \end{bmatrix} \alpha(\delta) + \begin{bmatrix} d_3 & d_4 \cos(\phi_1 - \phi_2) \\ d_4 \cos(\phi_1 - \phi_2) & d_5 \end{bmatrix} \begin{bmatrix} \ddot{\phi}_1 \\ \ddot{\phi}_2 \end{bmatrix} \quad \text{Eq. 9} \\ & + \begin{bmatrix} 0 & d_4 \sin(\phi_1 - \phi_2) \phi_2 \\ d_4 \sin(\phi_1 - \phi_2) \phi_1 & 0 \end{bmatrix} \begin{bmatrix} \dot{\phi}_1 \\ \dot{\phi}_2 \end{bmatrix} \\ & + \begin{bmatrix} -f_1 \sin(\phi_1) \\ -f_2 \sin(\phi_2) \end{bmatrix} \\ & + \begin{bmatrix} K_{pelvis}(\phi_1 - \phi_2) + C_{pelvis}(\dot{\phi}_1 - \dot{\phi}_2) \\ -K_{pelvis}(\phi_1 - \phi_2) - C_{pelvis}(\dot{\phi}_1 - \dot{\phi}_2) \end{bmatrix} = \begin{bmatrix} 0 \\ T_\phi \end{bmatrix} \end{aligned}$$

The crucial difference between Eq. 9 and the corresponding equation for the DCPC is that $\alpha(\delta)$ replaces the acceleration of the cart. The constants in Eq. 9 are defined as follows:

$$\begin{aligned} d_1 &= m_1 l_1 + m_2 L_1 & \text{Eq. 10} \\ d_2 &= m_2 l_2 \\ d_3 &= m_1 l_1^2 + m_2 L_1^2 + I_1 \\ d_4 &= m_2 L_1 l_2 \\ d_5 &= m_2 l_2^2 + I_2 \\ f_1 &= (m_1 l_1 + m_2 L_1)g \\ f_2 &= (m_2 l_2)g \end{aligned}$$

The constants m_1 , L_1 , l_1 and I_1 are, respectively, the mass, the length, the CoM ($L_1/2$) and the mass moment of inertia of the double pendulum's first rod, which represents the bicycle and the rider's lower body. The constants m_2 , L_2 , l_2 and I_2 are defined in the same way, but now for the second rod, which represents the rider's upper body. Further, g is the gravitational constant, and K_{pelvis} , C_{pelvis} and T_ϕ are the stiffness, the damping and the torque at the hips.

The SDP EoM are obtained from Eq. 8 and Eq. 9 by deriving expressions for the second derivatives $\ddot{\delta}$ and $[\ddot{\phi}_1, \ddot{\phi}_2]^T$. These expressions are complicated and not insightful. I use these EoM to define the state-space equations $\dot{\mathbf{x}} = \Omega(\mathbf{x}, \mathbf{u} + \mathbf{m})$ for the state variables $\mathbf{x} = [\delta, \phi_1, \phi_2, \dot{\delta}, \dot{\phi}_1, \dot{\phi}_2]^T$, external forces $\mathbf{u} = [T_\delta, T_{\phi_2}]^T$, and motor noise \mathbf{m} .

An optimal linear approximation of the SDP EoM

In our model for sensorimotor control, the computational system is a linear approximation of $\Omega(\mathbf{x}, \mathbf{u})$. I find an optimal linear approximation by calculating the Jacobian of $\Omega(\mathbf{x}, \mathbf{u})$ at the unstable fixed point $\mathbf{x} = \mathbf{0}$ and without external input (i.e., $\mathbf{u} = \mathbf{0}$). I obtained this Jacobian using the Matlab function `jacobian.m`. By taking the Jacobian of $\Omega(\mathbf{x}, \mathbf{u})$ with respect to \mathbf{x} and \mathbf{u} , I obtain, respectively, the matrices A and B . This allows for the following approximation near the unstable fixed point:

$$\dot{\mathbf{x}} \approx A\mathbf{x} + B\mathbf{u}$$

I numerically evaluated the accuracy of this approximation by calculating finite differences $[\Phi(\boldsymbol{\varepsilon}, \mathbf{0}) - \Phi(\mathbf{0}, \mathbf{0})]/\boldsymbol{\varepsilon}$ (for A) and $[\Phi(\mathbf{0}, \boldsymbol{\varepsilon}) - \Phi(\mathbf{0}, \mathbf{0})]/\boldsymbol{\varepsilon}$ (for B) for decreasing values of $\boldsymbol{\varepsilon}$. I found that for $\boldsymbol{\varepsilon} \rightarrow \mathbf{0}$ the finite difference approximations converged to A and B .

Realistic constants for the SDP

The dynamics of the SDP depends on a number of constants, and I will now determine realistic values for these constants.

Stiffness, damping and mass moment of inertia for the steering model

To assign realistic values to the stiffness and damping parameters of the steering model, it is useful to divide both sides of Eq. 8 by K_{steer} and to reparametrize the model as follows:

$$\tau^2 \ddot{\delta} + 2\zeta\tau \dot{\delta} + \delta = \frac{T_\delta}{K_{steer}} \quad , \quad \text{Eq. 11}$$

in which ζ is the damping ratio and τ is the time constant. Equating corresponding parts in Eq. 8 and Eq. 11, I obtain

$$K_{steer} = \frac{I_{steer}}{\tau^2} \quad \text{Eq. 12}$$

$$C_{steer} = 2\zeta\tau \quad \text{Eq. 13}$$

For a damping ratio $\zeta < 1$ the steering assembly oscillates in response to torque input. Because this does not happen in reality, ζ must be at least 1. The smaller the damping ratio ζ , the faster the response of the steering assembly, which is advantageous for stabilization. I will consider the most responsive steering assembly, and therefore set ζ to 1.

I now set the time constant τ to an empirically determined value. For that, I make use of the fact that a speeded single joint movement governed by a second order system reaches its maximum speed τ seconds after the beginning of the movement (see *Empirical determination of the time constant of a critically damped second order system*). From visual inspection of Figure 3B in Lewis & Perrault (2009), I estimate $\tau \approx 0.33$ seconds. From Eq. 13, I find that, in the critically damped case, C_{steer} equals 2τ .

The mass moment of inertia I_{steer} has two components, one determined by the bicycle's front assembly (I_{steer_bic}), and one by the rider's arms (I_{steer_arms}). I_{steer_bic} was calculated using measurements of Moore, Hubbard (38). These authors estimated the moment of inertia tensor of the front assembly (fork plus handlebars) and the wheel. This estimated tensor was for a fork with a 68.5 degrees steering axis, whereas for the SDP this is 90 degrees. I therefore rotated the tensor over 21.5 degrees, and obtained a mass moment of inertia about the vertical axis equal to 0.1262 kg m². The mass moment of inertia of the front

wheel was found to be 0.08 kg m^2 [38], such that $I_{steer_bic} = 0.1262 + 0.08 = 0.2062 \text{ kg m}^2$.

The mass moment of inertia I_{steer_arms} results from the fact that the arm muscles must also move themselves plus the bones to turn the front assembly. I treat the arms as 4 kg point masses at the end of the handlebars (turn radius 0.4 m.). It follows that $I_{steer_arms} = 2 \times 4 \times 0.4^2 = 1.28 \text{ kg m}^2$. Thus,

$$I_{steer} = I_{steer_bic} + I_{steer_arms} = 0.2062 + 1.28 = 1.2862 \text{ kg m}^2$$

Stiffness, damping and mass moment of inertia for the hips

I follow the same reasoning as for the steering model, and I also set the damping ratio $\zeta = 1$ and the time constant $\tau = 0.33$. The mass moment of inertia for the hip joint depends on the geometry and the mass of the model for the upper body, which I describe in the next paragraph.

Lengths and masses of the bicycle and upper body models

The SDP models the bicycle (plus lower body) and the upper body as rods. I consider a 15 kg. bicycle and a 85 kg. rider with a 45%-55% mass distribution between the lower and the upper body. The bicycle (lower body) height is 1.1 m., and the upper body height is 0.75 m. In terms of the constants in Eq. 10:

$$m_1 = (0.45 \times 85) + 15 = 53 \text{ kg}$$

$$m_2 = 0.55 \times 85 = 47 \text{ kg}$$

$$L_1 = 1.1 \text{ m}$$

$$L_2 = 0.75 \text{ m}$$

Using the formula for the mass moment of inertia of a homogeneous rod, I obtain

$$I_1 = \frac{m_1 L_1^2}{12} = 5.34 \text{ kg m}^2$$

$$I_2 = \frac{m_2 L_2^2}{12} = 2.2031 \text{ kg m}^2$$

Bicycle geometry

Our kinematic model depends on two constants: W , the wheelbase, and w_r , the combined CoG on the LoS. I find values for these constants in Table 8 and Eq. 8 of Moore, Hubbard (38):

$$\begin{aligned} W &= 1.12 \text{ m} \\ w_r &= 0.291 \text{ m} \end{aligned}$$

Gravity and speed

I set the gravitational constant $g = 9.81 \text{ m/sec}^2$, and the bicycle speed $v = 4.3 \text{ m/sec}$, the average bicycle speed in Copenhagen [39].

Empirical determination of the time constant of a critically damped second order system

I will now show that the time constant τ of a critically damped second order system can be determined empirically from an experiment in which participants make speeded movements of the joint that is modeled by this system. I start from the step response of this critically damped system:

$$\delta(t) = \frac{1}{K_{steer}} \left[1 - \left(1 + \frac{t}{\tau} \right) e^{-t/\tau} \right]$$

Using Eq. 12, I can replace K_{steer} by I_{steer}/τ^2 , such that I obtain

$$\delta(t) = \frac{\tau^2}{I_{steer}} \left[1 - \left(1 + \frac{t}{\tau} \right) e^{-t/\tau} \right]$$

Our objective is to find the time at which the angular rate $\dot{\delta}(t)$ is the highest. This angular rate is the following:

$$\dot{\delta}(t) = \frac{\partial \delta}{\partial t} = \frac{t e^{-t/\tau}}{I_{steer}} \propto t e^{-t/\tau}$$

The strictly monotone transformation $\ln(\dot{\delta}(t))$ is a concave function of t , and therefore the maximum of $\dot{\delta}(t)$ can be found by solving

$$\frac{\partial \ln(\dot{\delta}(t))}{\partial t} = 0$$

The result of this equation is $t = \tau$. Thus, the time constant τ is the time after movement onset at which the speed is the highest.

Simulating the stabilization of the mechanical by the computational system

I have written computer code in Matlab for simulating the stabilization of the mechanical by the computational system, and visualizing the results. This code is added to the supplementary material for this paper. With this code, one can perform all the simulations on which I have reported in this paper as well as variations inspired by one's own questions and hypotheses. Running simulations is only possible in discrete time, and I must therefore discretize the continuous time model. This is the main topic of this section.

Simulating the combined system in discrete time

The discrete time axis is defined by the increment Δt : $0, \Delta t, 2\Delta t, 3\Delta t \dots$. The model in Figure 3 involves a closed loop, and to describe it, one can start at every point. Here, I start from the sensory input system, which receives the state $\mathbf{x}(t)$ from the mechanical system, and feeds the noise-corrupted sensory input $\mathbf{y}(t) = \mathbf{C}\mathbf{x}(t) + \mathbf{s}(t)$ into the computational system. This is depicted schematically in Figure 9. The computational system determines the internal state estimate $\hat{\mathbf{x}}(t + \Delta t)$ on the basis of $\mathbf{y}(t)$, the previous internal state estimate $\hat{\mathbf{x}}(t - \Delta t)$, and the previous control action $\mathbf{u}(t - \Delta t)$. No internal state estimate is calculated for time t . The new control action $\mathbf{u}(t + \Delta t)$ is obtained from $\hat{\mathbf{x}}(t + \Delta t)$. Adding the motor noise $\mathbf{m}(t + \Delta t)$ to $\mathbf{u}(t + \Delta t)$ produces $\mathbf{z}(t + \Delta t)$, the input to the mechanical system. This input $\mathbf{z}(t + \Delta t)$, together with the previous state $\mathbf{x}(t)$ produces the new state $\mathbf{x}(t + 2\Delta t)$. From this new state and the sensor noise $\mathbf{s}(t + 2\Delta t)$, the new sensory input $\mathbf{y}(t + 2\Delta t)$ is obtained, which closes the loop. No actual state and sensory input is calculated at time $t + \Delta t$.

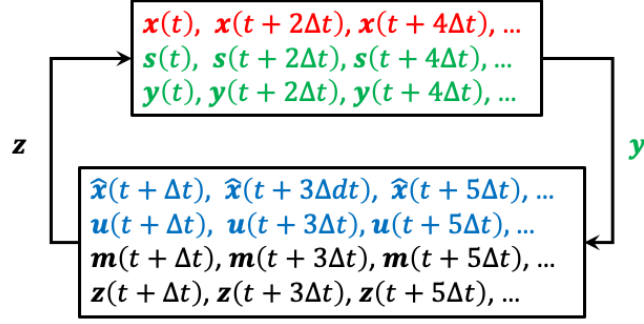


Figure 9: Schematic representation of the simulation of the combined system in discrete time. In red, green, blue and black, I show the variables that generated in, respectively, the mechanical, the sensory input, the computational, and the motor output system.

Solving the discrete time computational and mechanical system

For simulating the combined system, one must solve the discrete time mechanical and computational system. For the mechanical system, this involves finding $\mathbf{x}(t + 2\Delta t)$ by numerically integrating $\dot{\mathbf{x}} = \Omega(\mathbf{x}, \mathbf{z}) = \Omega(\mathbf{x}, \mathbf{u} + \mathbf{m})$ over the interval $[t, t + 2\Delta t]$ starting from the initial condition $\mathbf{x}(t)$ and with external input $\mathbf{u} = \mathbf{u}(t + \Delta t)$ and $\mathbf{m} = \mathbf{m}(t + \Delta t)$. For this, I used the Matlab function `ode45`, which is based on an explicit Runge-Kutta (4,5) formula [40].

To solve the discrete time computational system, I follow a similar approach, but now take advantage of the fact that an explicit solution exists for linear systems. Using this explicit solution, I can write the discrete time version of the linear approximation as follows:

$$\mathbf{x}(t + \Delta t) = A_{2\Delta t}\mathbf{x}(t - \Delta t) + B_{2\Delta t}\mathbf{u}(t - \Delta t) + \Sigma_{2\Delta t}^{1/2}\mathbf{n}^{(1)} \quad \text{Eq. 14}$$

$$\mathbf{y}(t) = C_{2\Delta t}\mathbf{x}(t - \Delta t) + \Psi_{2\Delta t}^{1/2}\mathbf{n}^{(2)} \quad \text{Eq. 15}$$

The simulated versions of the actual motor and sensor noise are, respectively, $\Sigma_{2\Delta t}^{1/2}\mathbf{n}^{(1)}$ and $\Psi_{2\Delta t}^{1/2}\mathbf{n}^{(2)}$, with $\mathbf{n}^{(1)}$ and $\mathbf{n}^{(2)}$ denoting independent normally distributed random variables with an identity covariance matrix. The noises $\Sigma_{2\Delta t}^{1/2}\mathbf{n}^{(1)}$ and $\Psi_{2\Delta t}^{1/2}\mathbf{n}^{(2)}$ thus have a normal distribution with respective covariance matrices $\Sigma_{2\Delta t}$ and $\Psi_{2\Delta t}$, which are defined as follows:

$$\Sigma_{2\Delta t} = \int_0^{2\Delta t} e^{A\tau} \Sigma e^{A^T \tau} d\tau$$

$$\Psi_{2\Delta t} = (2\Delta t)\Psi$$

The matrices $A_{2\Delta t}$, $B_{2\Delta t}$, and $C_{2\Delta t}$ follow from the well-known solution of a linear state-space model with defining matrices A , B , and C : $A_{2\Delta t} = e^{A(2\Delta t)}$, $B_{2\Delta t} = A^{-1}(A_{2\Delta t} - I)B$, and $C_{2\Delta t} = C$ [41]. Note that the sensory input \mathbf{y} (see Figure 9) is evaluated at a different time than the simulated state variable \mathbf{x} , because the former is obtained from the mechanical system.

In one of the simulation studies (*Is the optimal model good enough to balance a bicycle under realistic conditions?*), I used the optimal learned motor and sensor noise covariance matrices $\Sigma_{2\Delta t}$ and $\Psi_{2\Delta t}$. For the continuous time case, these optimal learned noise covariance matrices are the following functions of the actual noise covariance matrices Φ and Ξ : $\Sigma = B\Phi B^T$ and $\Psi = \Xi$. For the discrete time case, the corresponding formulas are the following:

$$\Sigma_{2\Delta t} \approx \int_0^{2\Delta t} e^{A\tau} B\Phi B^T e^{A^T \tau} d\tau$$

$$\Psi_{2\Delta t} = (2\Delta t)\Xi$$

For the discrete time computational system in Eq. 14 and Eq. 15, I calculate control actions \mathbf{u} that minimize a cost functional $J_{2\Delta t}$:

$$J_{2\Delta t} = \lim_{N \rightarrow \infty} \frac{1}{N} \mathcal{E} \left(\sum_{n=1}^N [\mathbf{x}(n2\Delta t - \Delta t)' Q \mathbf{x}(n2\Delta t - \Delta t) + \mathbf{u}(n2\Delta t - \Delta t)' R \mathbf{u}(n2\Delta t - \Delta t)] \right)$$

The cost functional $J_{2\Delta t}$ is minimized by control actions $\mathbf{u} = -M_{2\Delta t} \hat{\mathbf{x}}$, in which $-M_{2\Delta t}$ is the discrete time LQR gain (which depends on the matrices $A_{2\Delta t}$, $B_{2\Delta t}$, Q , and R), and $\hat{\mathbf{x}}$ is the optimal state estimate defined by this discrete time ODE:

$$\hat{\mathbf{x}}(t + \Delta t) = (A_{2\Delta t} - B_{2\Delta t} M) \hat{\mathbf{x}}(t - \Delta t) + K_{2\Delta t} [\mathbf{y}(t) - C_{2\Delta t} \hat{\mathbf{x}}(t - \Delta t)] \quad \text{Eq. 16}$$

The matrix $K_{2\Delta t}$ is the discrete time Kalman gain, which depends on $A_{2\Delta t}$, $C_{2\Delta t}$, $\Sigma_{2\Delta t}$, and, $\Psi_{2\Delta t}$.

Discrete time motor and sensor noise

From the properties of a Wiener process, it is straightforward to obtain the discrete time motor and sensor noise from the continuous time equations Eq. 1 and Eq. 2:

$$\mathbf{z}(t + \Delta t) = \mathbf{u}(t + \Delta t) + \Phi_{2\Delta t}^{1/2} \mathbf{n}^{(1)} \quad \text{Eq. 17}$$

$$\mathbf{y}(t) = \mathbf{C}\mathbf{x}(t) + \Xi_{2\Delta t}^{1/2} \mathbf{n}^{(2)} \quad \text{Eq. 18}$$

The noises $\Phi_{2\Delta t}^{1/2} \mathbf{n}^{(1)}$ and $\Xi_{2\Delta t}^{1/2} \mathbf{n}^{(2)}$ have a normal distribution with respective covariance matrices $\Phi_{2\Delta t} = (2\Delta t)\Phi$ and $\Xi_{2\Delta t} = (2\Delta t)\Xi$.

References

1. Todorov E. Optimality principles in sensorimotor control. *Nature neuroscience*. 2004;7(9):907-15.
2. Todorov E, Jordan MI. Optimal feedback control as a theory of motor coordination. *Nature neuroscience*. 2002;5(11):1226-35.
3. Franklin DW, Wolpert DM. Computational mechanisms of sensorimotor control. *Neuron*. 2011;72(3):425-42.
4. Wolpert DM, Ghahramani Z, Flanagan JR. Perspectives and problems in motor learning. *Trends in cognitive sciences*. 2001;5(11):487-94.
5. Dong O, Graham C, Grewal A, Parrucci C, Ruina A. The bricycle: a bicycle in zero gravity can be balanced or steered but not both. *Vehicle system dynamics*. 2014;52(12):1681-94.
6. Meijaard JP, Papadopoulos JM, Ruina A, Schwab AL, editors. *Linearized dynamics equations for the balance and steer of a bicycle: a benchmark and review*. Proceedings of the Royal Society of London A: Mathematical, Physical and Engineering Sciences; 2007: The Royal Society.
7. Cain SM, Ashton-Miller JA, Perkins NC. On the skill of balancing while riding a bicycle. *PLoS one*. 2016;11(2):e0149340.
8. Bogdanov A. Optimal control of a double inverted pendulum on a cart. Oregon Health and Science University, Tech Rep CSE-04-006, OGI School of Science and Engineering, Beaverton, OR. 2004.
9. Tedrake R. *Underactuated Robotics: Algorithms for Walking, Running, Swimming, Flying, and Manipulation (Course Notes for MIT 6.832)*. Downloaded on 20-08-2021 from <http://underactuated.mit.edu/>. 2021.
10. Kooijman J, Meijaard JP, Papadopoulos JM, Ruina A, Schwab A. A bicycle can be self-stable without gyroscopic or caster effects. *Science*. 2011;332(6027):339-42.
11. Todorov E. Stochastic optimal control and estimation methods adapted to the noise characteristics of the sensorimotor system. *Neural computation*. 2005;17(5):1084-108.
12. Yeo S-H, Franklin DW, Wolpert DM. When optimal feedback control is not enough: Feedforward strategies are required for optimal control with active sensing. *PLoS computational biology*. 2016;12(12):e1005190.
13. Nagengast AJ, Braun DA, Wolpert DM. Optimal control predicts human performance on objects with internal degrees of freedom. *PLoS computational biology*. 2009;5(6):e1000419.
14. Nagengast AJ, Braun DA, Wolpert DM. Risk-sensitive optimal feedback control accounts for sensorimotor behavior under uncertainty. *PLoS computational biology*. 2010;6(7):e1000857.
15. Faisal AA, Selen LP, Wolpert DM. Noise in the nervous system. *Nat Rev Neurosci*. 2008;9(4):292-303. doi: 10.1038/nrn2258. PubMed PMID: 18319728; PubMed Central PMCID: PMC2631351.
16. Åström KJ. *Introduction to stochastic control theory*: Courier Corporation; 2012.
17. Wolpert DM, Ghahramani Z, Jordan MI. An internal model for sensorimotor integration. *Science*. 1995;269(5232):1880-2.
18. Körding KP, Wolpert DM. Bayesian integration in sensorimotor learning. *Nature*. 2004;427(6971):244-7.

19. Saunders JA, Knill DC. Visual feedback control of hand movements. *Journal of Neuroscience*. 2004;24(13):3223-34.
20. Shadmehr R, Mussa-Ivaldi FA. Adaptive representation of dynamics during learning of a motor task. *Journal of neuroscience*. 1994;14(5):3208-24.
21. Flanagan JR, Wing AM. The role of internal models in motion planning and control: evidence from grip force adjustments during movements of hand-held loads. *Journal of Neuroscience*. 1997;17(4):1519-28.
22. Flanagan JR, Lolley S. The inertial anisotropy of the arm is accurately predicted during movement planning. *Journal of Neuroscience*. 2001;21(4):1361-9.
23. Li C-SR, Padoa-Schioppa C, Bizzi E. Neuronal correlates of motor performance and motor learning in the primary motor cortex of monkeys adapting to an external force field. *Neuron*. 2001;30(2):593-607.
24. Gribble PL, Scott SH. Overlap of internal models in motor cortex for mechanical loads during reaching. *Nature*. 2002;417(6892):938-41.
25. Green M, Limebeer DJ. Linear robust control: Courier Corporation; 2012.
26. Rajamani R. Vehicle dynamics and control: Springer Science & Business Media; 2011.
27. Kitazawa S, Kimura T, Uka T. Prism adaptation of reaching movements: specificity for the velocity of reaching. *Journal of Neuroscience*. 1997;17(4):1481-92.
28. Desmurget M, Grafton S. Forward modeling allows feedback control for fast reaching movements. *Trends in cognitive sciences*. 2000;4(11):423-31.
29. Miall RC, Weir DJ, Wolpert DM, Stein J. Is the cerebellum a smith predictor? *Journal of motor behavior*. 1993;25(3):203-16.
30. Wolpert DM, Kawato M. Multiple paired forward and inverse models for motor control. *Neural networks*. 1998;11(7-8):1317-29.
31. Crevecoeur F, Gevers M. Filtering compensation for delays and prediction errors during sensorimotor control. *Neural computation*. 2019;31(4):738-64.
32. Crevecoeur F, Munoz DP, Scott SH. Dynamic multisensory integration: somatosensory speed trumps visual accuracy during feedback control. *Journal of Neuroscience*. 2016;36(33):8598-611.
33. Crevecoeur F, Scott SH. Priors engaged in long-latency responses to mechanical perturbations suggest a rapid update in state estimation. *PLoS computational biology*. 2013;9(8):e1003177.
34. Schmidt RA, Zelaznik H, Hawkins B, Frank JS, Quinn Jr JT. Motor-output variability: a theory for the accuracy of rapid motor acts. *Psychological review*. 1979;86(5):415.
35. Todorov E. Cosine tuning minimizes motor errors. *Neural computation*. 2002;14(6):1233-60.
36. Phillis Y. Controller design of systems with multiplicative noise. *IEEE Transactions on Automatic Control*. 1985;30(10):1017-9.
37. Phillis Y. A smoothing algorithm for systems with multiplicative noise. *IEEE transactions on automatic control*. 1988;33(4):401-3.
38. Moore JK, Hubbard M, Kooijman J, Schwab A, editors. A method for estimating physical properties of a combined bicycle and rider. *International Design Engineering Technical Conferences and Computers and Information in Engineering Conference*; 2009.
39. "Bicycle statistics". City of Copenhagen website.: City of Copenhagen; 2013 [Archived from the original on 12 December 2013. Retrieved 12 December 2013.].

40. Shampine LF, Reichelt MW. The matlab ode suite. SIAM journal on scientific computing. 1997;18(1):1-22.
41. DeCarlo RA. Linear systems: A state variable approach with numerical implementation: Prentice-Hall, Inc.; 1989.

Supporting information

- StabSDPusingLQG_3.mlx. Matlab live script for simulating the stabilization of the mechanical by the computational system, and visualizing the results.
- drawSDP.m. Matlab function called by StabSDPusingLQG_3.mlx.
- evaldeqSDP.m. Matlab function called by StabSDPusingLQG_3.mlx.
- d2DCPS.m. Matlab function called by StabSDPusingLQG_3.mlx.
- d2steer.m. Matlab function called by StabSDPusingLQG_3.mlx.
- cfacc.m. Matlab function called by StabSDPusingLQG_3.mlx.

Figure captions

Figure 1: Kinematic variables of the bicycle model plus the rider-controlled torques. (A) Side view. In green, the bicycle rear frame, characterized by its lean angle ϕ_1 over the roll axis (green arrow). In red, the bicycle front frame, characterized by its angle δ over the steering axis (red arrow). In blue, the rider's upper body, characterized by its lean angle ϕ_2 over the roll axis (blue arrow). In black, (1) the steering torque T_δ and the lean torque T_{ϕ_2} , which are both applied by the rider, and (2) the steering axis angle λ , which is set equal to 90 degrees for the purposes of the present paper (see text). (B) Rear view. In green, the bicycle rear frame (plus lower body) lean angle ϕ_1 (which is equals the front frame lean angle). In blue, the rider's upper body lean angle ϕ_2 . The symbol \otimes denotes the CoG of the upper body (in blue), the lower body (in green), and combined (in black).

Figure 2: Bicycle model without the known factors that affect bicycle self-stability. Compared to Figure 1, this model has ice skates instead of wheels and a vertical steering axis.

Figure 3: Sensorimotor control of a mechanical system (in red) by input from a computational system (in blue). The mechanical system is governed by the nonlinear differential equations $\dot{\mathbf{x}} = \Omega(\mathbf{x}, \mathbf{z})$, and the computational system produces an optimal control action \mathbf{u} . The motor output system (in black) adds noise \mathbf{m} to \mathbf{u} and feeds this into the mechanical system. The sensory input system (in green) maps the state variables \mathbf{x} to sensory variables, adds noise \mathbf{s} and feeds the resulting sensory input \mathbf{y} into the computational system. The computational system calculates an optimal internal state estimate $\hat{\mathbf{x}}$ by integrating a linear differential equation (characterized by the matrices A , B , C , and the Kalman gain K) that takes the sensory feedback \mathbf{y} as input. The optimal control action \mathbf{u} is obtained from $\hat{\mathbf{x}}$ and the LQR gain $-M$.

Figure 4: Maximum absolute (MaxAbs) steering angle, combined CoG lean angle, and steering angular rate as a function of the noise level in the simulation. In the

left panel, I show the average MaxAbs over all simulated trials, and in the right panel I show the average MaxAbs averaged separately over the completed and interrupted trials. In this simulation, the Kalman and the LQR gain were calculated at the optimal learned parameter values (see text).

Figure 5: Maximum absolute (MaxAbs) steering angle, combined CoG lean angle, and steering angular rate as a function of the learned motor (top row) and the learned sensor noise level fraction (bottom row). Across all simulations, the actual noise amplitude was kept constant; only the learned noise covariance matrices were manipulated. Both the learned motor noise (top row) and the learned sensor noise (bottom row) were set equal to a fraction of the actual noise amplitude, with the fraction ranging from 0.1 to 10, and logarithmically spaced. In the left panels, I show the average MaxAbs over all simulated trials, and in the right panels I show the average MaxAbs averaged separately over the completed and the interrupted trials.

Figure 6: Element-wise ratio of the Kalman gain matrices for the largest and the smallest learned motor noise level fraction (noise level fraction 10 over 0.1). The tick labels for the state and the sensor variable are identical because the defining matrix for the sensory system (C) is the identity matrix.

Figure 7: Maximum absolute (MaxAbs) steering angle, combined CoG lean angle, and steering angular rate as a function of the learned speed fraction. Across all simulations, the actual speed was kept constant; only the learned speed and the associated system matrix was manipulated. The learned speed was set equal to a fraction of between 0.85 and 1.15 of the actual speed. In the left panel, I show the MaxAbs averaged over all simulated trials, and in the right panel the MaxAbs averaged separately over the completed and the interrupted trials.

Figure 8: The relevant kinematic variables of the SPD in both an inertial (yellow origin) and a rider/bicycle-centered (purple origin) reference frame. The inertial reference frame has an arbitrary origin, and the rider/bicycle-centered reference frame has its origin at the orthogonal projection of the combined CoM on the LoS.

These reference frames have parallel coordinate axes. In green and blue, I depict the lean angles of the lower and the upper body (ϕ_1 and ϕ_2), and in red, I depict the yaw angle ψ of the LoS. The horizontal plane (road surface) is colored light yellow.

Figure 9: Schematic representation of the simulation of the combined system in discrete time. In red, green, blue and black, I show the variables that generated in, respectively, the mechanical, the sensory input, the computational, and the motor output system.